Feasibility study of an ATES triplet

Master Thesis

Abstract

Aquifer Thermal Energy Storages (ATES) are used to store hot or cold water in an aquifer, where the thermal energy of the water can be used at later times. This way, the discrepancy between a heating demand of buildings in winter and a cooling demand in summer can be overcome. In order to provide in heating and cooling demands, a heat pump is currently required to heat or cool a building at effective temperatures. In buildings with ATES doublet systems, the heat pump uses the most energy for space conditioning. An ATES system without a heat pump is proposed in this work by using three wells (triplet), solar heat collectors and a dry cooler. The solar heat collectors are used to inject water at 40°C in the warm storage when there is incoming solar radiation. Similarly, the dry cooler is used to inject water of 5°C in the cold storage when the air temperature is below 4°C. The feasibility of the ATES triplet is mostly affected by the thermal losses of the warm well, which are consequently influenced by: a) the ratio between the area and volume of the warm storage and b) the hydraulic conductivities in the aquifer. Apart from that, the weather conditions also have a great impact on the feasibility of an ATES triplet. The best conditions for the realization of an ATES triplet are buildings with a gross surface area over 40.000m^2 in temperate climate conditions on top of fine-sanded aquifers. By looking at a case scenario on the TU Delft campus, the triplet is shown to be feasible in a temperate marine climate like in the Netherlands and shows massive improvements in operational costs and CO_2 emissions. Investment costs of the ATES triplet are high compared to the investment costs of an ATES doublet or a conventional, gas-fired boiler system. The high investment costs are due to the high price of solar heat collectors and hence a high equity capital is required for the realization of an ATES triplet.

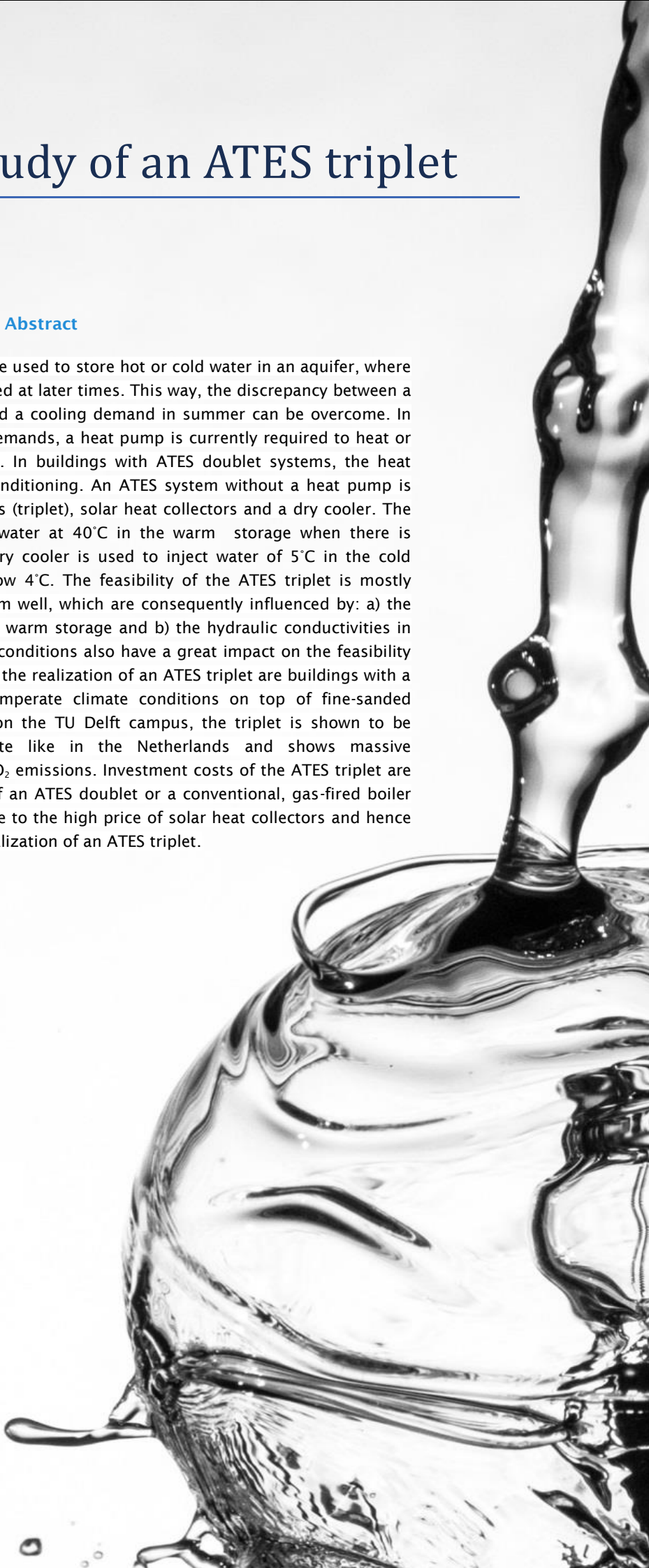

KWR Watercycle Research Institute

Feasibility study of an ATES triplet

Master thesis

KWR | April 2017

Author
Jan Jaap Pape

Supervisors
Niels Hartog[1,2]
Martin Bloemendal[1,3]
Majid Hassanzideh[2]

Cooperating institutions
[1]KWR Watercycle Research Institute
[2]Utrecht University
[3]TU Delft

Year of publishing
2017

More information
Jan Jaap Pape
T +31 628155676
E **Janjaappape@gmail.com**

PO Box 1072
3430 BB Nieuwegein
The Netherlands

T +31 (0)30 60 69 511
F +31 (0)30 60 61 165
E info@kwrwater.nl
I www.kwrwater.nl

KWR Watercycle Research Institute

Contents

1 Introduction

Introduction to the development of an ATES triplet

Increasing concerns about the negative consequences of climate change is causing an increasing demand for alternative sources of energy production and reducing current energy uses. This has consequences on the size and geographical distribution of renewable energy sources, but more research is necessary on the magnitude and applicability of using renewable energy (IPCC 2011). Particularly the energy use by buildings can be reduced and be made more sustainable. In this sector, the most energy is currently used to control the climate inside the building. The climate control is driven by the demand for heating and cooling and is realized by heating, ventilation, air conditioning and cooling (HVAC) systems (Pérez-Lombard et al. 2008). The demand for heating or cooling depends on incoming radiation, shading, wind and building materials, but mostly on the air temperature in the canopy layer. Therefore, in temperate climates like in the Netherlands, there will be a period with a heating demand and a period with a cooling demand. The temporal discrepancy between a cold and a warm season can be overcome by storing a medium with high temperatures in the warm season and with low temperatures in the cold season. By making use of solar radiation and the air temperature, the storage of this energy is completely sustainable and diminishes the energy use by buildings (Lee 2013).

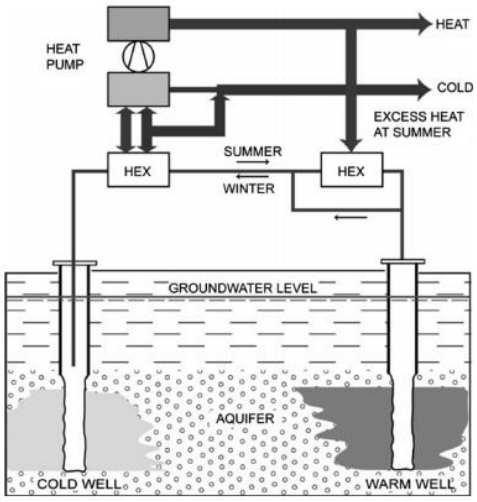

Figure 1: Conventional ATES system with a heat pump and two heat exchangers (HEX) *source: (Lee 2013)*

Aquifer thermal energy storage (ATES) systems are used to overcome the discrepancy between the heat demand in winter and the cold demand in summer, by using wells to store the thermal energy in aquifers (see Figure 1). In contrast to borehole thermal energy storage systems (BTES), which make use of a closed loop with a chemical fluid (typically glycol) pumped through the loop, ATES systems make use of the groundwater to carry the thermal energy from the underground storage. ATES systems are not only capable of storing more thermal energy compared to BTES systems, but are also shown to be more efficient (Lee 2013). For the realization of a typical ATES, two wells are drilled into the aquifer and placed at a distance so that the warm and cold storages do not interfere. The transfer of thermal energy is consequently carried out by discharging the cold or warm storage, pumping it through a heat exchanger and re-injecting it at a modified temperature in the other well (Lee 2010). The heat exchanger is necessary in order to make sure that the water in the aquifer and the fluid which is used for energy transfer in the building will not mix. Typically, ATES systems that supply both in heating and cooling demands use a heat pump to gain additional heating or cooling capacity (Rostampour et al. 2017). This additional energy is necessary to effectively cool or heat the space inside a building. Several heat release systems are identified for transferring thermal energy into the space of the building. Each system has its own benefits and varies in operative temperatures. For example, conventional systems such as a radiator, need approximately 80˚C for heating. In contrast to that, floor heating systems require 40˚C for effective heating and 10˚C for cooling. The lower effective

temperatures make the latter system more appropriate to use in combination with an ATES system because the temperature losses in the subsurface will be limited compared to higher storage temperatures. In addition, the efficiency of heating up the air in a room to 20˚C is higher with a temperature of 40˚C compared to heating with 80˚C (Bloemendal et al. 2013), which suits the purpose of a more sustainable energy provision. Eventually the energy savings achieved by storing the thermal energy, make ATES systems more sustainable than a conventional heating system with a boiler. Previous work has shown that the energy savings of ATES systems with a heat pump reach up to 60%-75% of the energy a conventional system would use (Paksoy et al. 2000).

Although the doublet ATES system is a good example of a renewable way of saving energy, even more energy can be saved compared to a conventional system. Research has shown that the heat pump is responsible for over 60% (Dekker 2016) of the energy used in a ATES-heat pump system (Figure 2). This raises the question if the efficiency of this system can further be improved by reducing the use of the heat pump or making it abundant. Using high temperature (HT) storages (temperatures above 80˚C), which can provide enough thermal energy to heat or cool buildings at peak demands is an option to further reduce the energy use of the system. The energy use is shown to be reduced and on top of that HT storages reduce the storage volumes with the same amount of thermal energy. However, there are very few examples of actual HT ATES applications, due to the problems with HT storages. The main problems are concerning precipitation of carbonates, enhanced corrosion of the piping and low storage efficiencies (Drijver 2013).

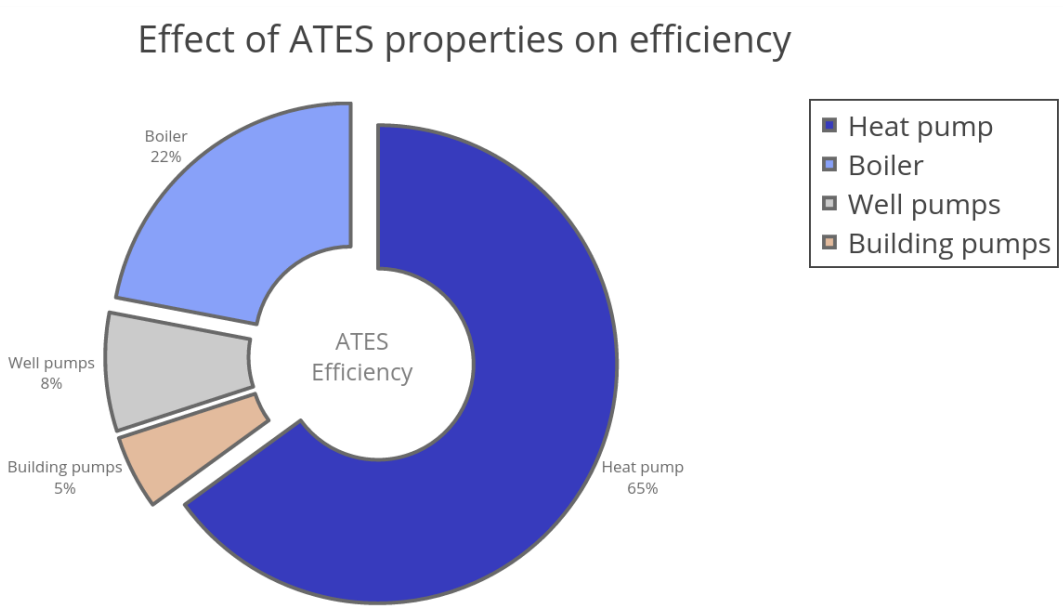

Figure 2: Efficiency of ATES doublet. *Source: (Dekker 2016)*

In order to minimize the problems concerning the HT ATES systems, but to maximize the potential for saving energy by cutting out the heat pump and by following the requirements for floor heating systems, storage temperatures of 40˚C can be used (Bloemendal et al. 2013). Sustainable ways of heating the water to 40˚C and cooling the water to 5˚C can be realized by installing solar heat collectors and a dry cooler at the roof of a building. The water can only be heated up when there is solar radiation and cooled down when the ambient air temperature is lower than 4˚C. So when there is no incoming solar radiation but there is a cooling demand, the water injected into the warm storage would in current ATES doublets cool the warm storage.

Therefore this research introduces a triple well ATES system (triplet) instead of a double well ATES system (doublet). The third storage or 'buffer storage' prevents 'pollution' of the warm and the cold storages at times when the weather conditions are unfavorable for either cooling or heating. In addition, the buffer storage can supply additional water to be heated or cooled when weather conditions are favorable for heating or cooling. Moreover, when there is no demand the warm and cold storages can also be charged from the

buffer storage. By making use of the three storages, the solar heat collectors and the dry cooler a space conditioning system is introduced which minimizes the energy use and maximizes the use of sustainable thermal energy resources. Apart from the pumping energy, the ATES triplet is fully self-supporting. The ATES triplet is therefore considered as a thermally self-supporting energy system.

1.1 Aims

To what extent a thermally self-supporting ATES system is feasible and under which conditions this system would be best applicable is still to be investigated. This research investigates the feasibility and the potential of an ATES triplet under different circumstances. So the main aim is expressed as:

What is the potential of a thermally self-supporting ATES triplet?

This potential is investigated by considering different properties of the ATES triplet and the effects these properties have on the performance. First of all, the potential is tested by comparing the building sizes and hence the storage volumes to the performance of the ATES triplet.

- 1. "How do building and storage volume sizes relate to the performance and applicability of an ATES triplet?"

Apart from the building sizes and storage volumes, the aquifer properties will have their impact on the performance as well. Hence the aquifer properties are examined with respect to the potential of the ATES triplet.

- 2. "How do aquifer properties affect the performance of an ATES triplet?"

Another main driver is the weather variability. Taking the expected climate change into account, the weather conditions are a factor which will influence the performance and installation costs of a triplet system. Therefore the following aspect is also considered:

- 3. "What climatologic conditions show potential for installing an ATES triplet?

Finally the potential is analyzed in terms of cuts in CO_2 emissions, operational costs and the total costs of a system over its lifespan (Figure 3). So the environmental and economic gains of an ATES triplet are compared to an ATES doublet and a conventional space conditioning, resulting in the final research question:

- 4. "What are the energetic, environmental and economic benefits of an ATES triplet compared to conventional space conditioning or an ATES doublet?"

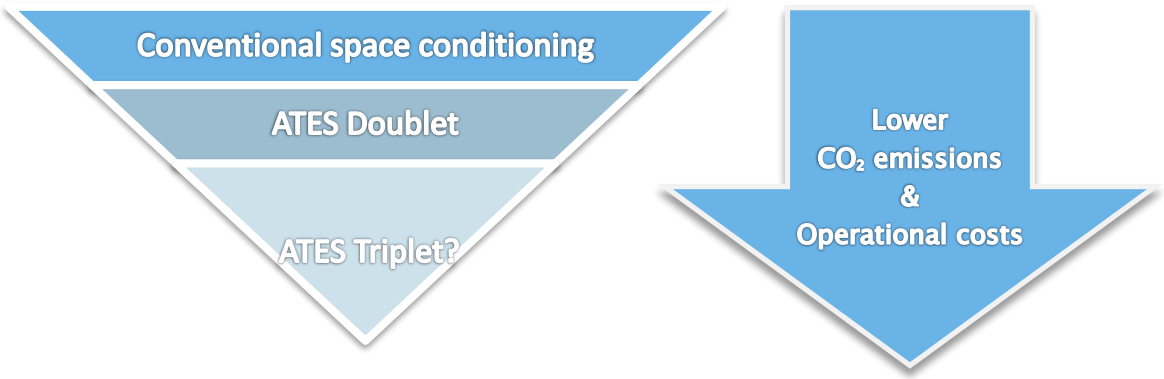

Figure 3: Hypothesis on the environmental and economic performance of an ATES triplet.

2 ATES triplet

A description of the ATES triplet, its properties and the main drivers of the system.

2.1 ATES triplet concept

The ATES triplet is aimed to provide in the heating and cooling demand of a building by making use of three storages in the subsurface; a warm, cold and buffer storage. When there is a heating demand, the warm storage can provide in a heat demand by using the warm water directly in the heat exchanger of the building. Similarly the water from the cold storage can be used to directly to cool the building. Following the requirements of floor heating systems, the warm storage is injected with water of 40˚C, the cold storage with water of 5˚C and the buffer storage is injected with water coming out of the heat exchanger of the building. The water going into the warm storage can be heated by solar heat collectors at the roof of a building and the water going into the cold storage can be cooled by a dry cooler. The concept and its properties are schematically shown in Figure 4, where a heating demand is considered.

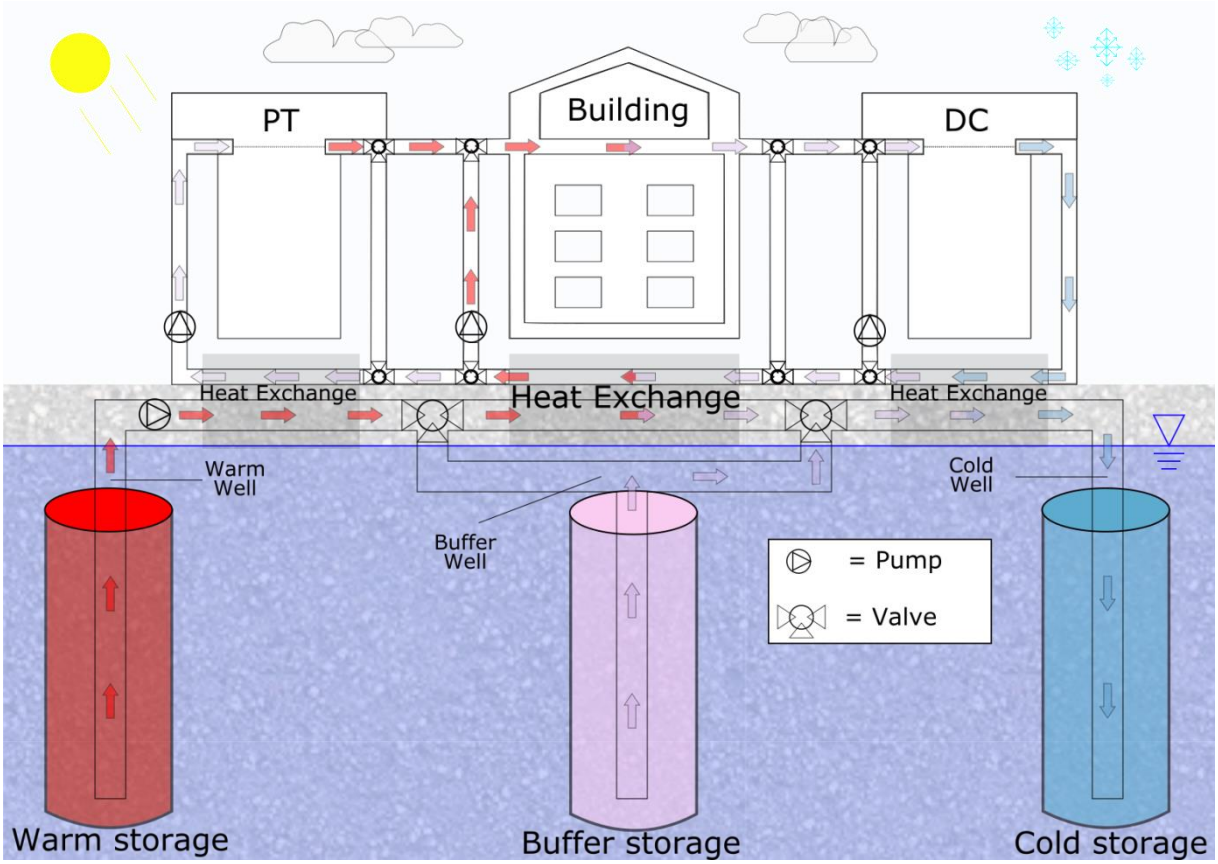

Figure 4: Conceptual visualization of an ATES triplet system (cold season). PT is the (photo-thermic) solar heat collector, DC stands for the dry cooler. The setting of the valves and the direction of the pumping is determined by the operating modes.

2.1.1 Heating demand

In order to maximize the use of the solar heat collectors, the heat produced by the solar heat collectors can directly be used by the building. Therefore three different scenarios can be distinguished in order to provide in the heating demand:

- When the thermal energy produced by the solar heat collectors is exactly enough to cover the heat demand, pumping from the warm storage is not needed.

- At times when the thermal energy produced by the solar heat collectors is more than the heating demand, the buffer storage can supply water to the solar heat collectors in order to charge the warm storage.
- When the produced thermal energy by the solar heat collectors is not covering the heating demand, the warm storage can supply additional heat to the building.

In the latter case the water pumped from the warm storage is carried through the heat exchanger of the building, after which it is assumed to have a temperature of 25°C. This water can be used to charge to the cold storage, or is pumped to the buffer storage.

2.1.1.1 Charging cold storage

In order to inject the water in the cold well at 5˚C and by assuming that the dry cooler incorporates some losses, the ambient air temperature is required to be lower than 4˚C. When this condition is met, the cold storage can be charged according to the capacity of the dry cooler. The following scenarios can then be identified:

- If the capacity of the dry cooler is higher than the capacity to cool down the water coming from the warm storage, additional water from the buffer storage can be supplied to the dry cooler (this is the case in Figure 4).
- When the capacity of the dry cooler is lower than the capacity to cool down the water coming from the warm storage, the maximum capacity of the dry cooler is used to inject cold water in the cold well. The surplus of water coming from the warm storage is then pumped into the buffer well.

2.1.2 Cooling demand

Contrary to providing in a heating demand, the only way to provide in a cooling demand is by using the water from the cold storage. The water is carried through the heat exchanger of the building, after which it is assumed to have a temperature of 15˚C. The water is than either used to charge the warm storage or pumped into the buffer well.

2.1.2.1 Charging warm storage

The warm storage is charged according to the capacity of the solar heat collectors, which depends on the incoming solar radiation. When there is a cooling demand and there is incoming solar radiation, the following scenarios can be identified for charging the warm storage:

- When the capacity of the solar heat collectors is higher than the capacity to heat all the water coming from the cold storage, additional water from the buffer storage can be supplied to the solar heat collectors.
- When the capacity of the solar heat collectors is lower than the capacity to heat all the water coming from the cold storage, the maximum capacity of the solar heat collectors is used to charge the warm storage. To prevent the warm storage from cooling, the surplus of water coming from the cold storage is pumped into the buffer well.

2.1.3 No heating or cooling demand

When there is no demand for heating or cooling (e.g. during night times) the cold and warm storage are further charged, provided that the conditions for charging the storages are met. The charging can be realized by pumping water from the buffer storage to the dry cooler and the solar heat collector. Note that the warm and cold storage can be charged simultaneously.

2.1.4 Maximum thermal energy

A maximum thermal energy is introduced to prevent inefficient pumping. To illustrate this, consider the following; when the warm storage reaches a certain level of thermal energy, there is enough capacity to provide in the heat demand for the upcoming cold season. This level is dictated by the average yearly heating or cooling demand times a safety factor which has to make sure the capacity is sufficient for an extreme upcoming cold or warm season. The safety factor f_{max} is empirically determined and is estimated to be 1.5 times the yearly heat or cool demand. When this level is reached, it is inefficient to pump more warm water into the warm well. In addition, if there was no limit on the amount of thermal energy in the warm or cold

storage, the storages keep on expanding and will start to influence each other. Therefore the warm and cold storages are not charged when they reach their level of maximum thermal energy.

2.1.5 Operating modes

The conditions described in section 2.1.1 to 2.1.4 dictate the operating mode of the ATES triplet. The operating mode can also be expressed by a set of switches which determine which storages are charged and discharged. The switches are:

$$s_{dd}^{i}, s_{dd,w}^{i} \in \{-1, 0, 1\} \quad (1)$$

$$s_{wc}^{i}, s_{wb}^{i}, s_{cb}^{i} \in \{0, 1\} \quad (2)$$

Where s_{dd} is the pumping direction operating mode which indicates if the system discharges the warm storage/charges the cold storage (-1), is not pumping (0) or charges the warm storage/discharges the cold storage (1). The $s_{dd,w}^{i}$ indicates when during a heat demand the warm storage is charged (1) or discharged (-1). The $s_{wc}^{i}, s_{wb}^{i}\ and\ s_{cb}^{i}$ switches indicate the interaction between the storages (warm $_w$, cold $_c$ or buffer $_b$). There is either volume pumped between the storages (1) or there is no interaction (0). As an illustration, consider the scenario with a heating demand in Figure 4. This leads to $s_{dd} = -1$, because the warm storage is discharged and the cold storage is charged. There is interaction between the warm and cold storage and between the buffer and cold storage so $s_{wc} = 1$, $s_{wb} = 0$ and $s_{cb} = 1$. An overview of the conditions leading to different sets of switches can be found in Appendix B.

2.1.6 Starting up

In order to start the ATES triplet, a season is picked with mostly cooling demands. In temperate climates, like in the Netherlands, the ambient groundwater of 11˚C is assumed to be cold enough to provide effective cooling. Hence the warm storage can be charged for the upcoming colder season and the system does not require alternative (non-sustainable) sources for heating or cooling.

2.2 Solar heat collectors

Several studies have been performed on the efficiency of a solar heat collector with varying designs and heat transfer elements, e.g. (Mathioulakis et al. 2002). In this study the flat plate solar collector with an integrated heat pipe is considered to provide the additional heat (see Figure 5a). The heat is collected by an absorber plate which consequently heats up liquid ethanol. The ethanol is situated below the absorber plate and may freely move through the piping. Because ethanol has a low boiling point it starts to evaporate relatively quick compared to water. The vapor is carried to the upper collector pipe where the ethanol condensates and heats up the water inside the pipe. In domestic applications the water is subsequently pumped to a storage reservoir where the heated water is stored until further use. In this study the water will be pumped into the warm well.

The efficiency of solar heat collector may be described as the amount of heat transferred to the water divided by the total incoming solar heat in the same time period (Wei et al. 2013):

$$\eta = \frac{m_w \cdot c_{p,w} \cdot \Delta T_w}{A \int_0^{\Delta t} G \cdot dt} \quad (3)$$

Where $m_w(kg)$ is the mass of the water, $c_{p,w}(J \cdot kg^{-1} \cdot K^{-1})$, $\Delta T_w(K)$ is the temperature difference, $A(m^2)$ the area of incidence and $G(W \cdot m^{-2})$ the incoming solar radiation. Research on this type of solar heat collector has shown that the efficiency could reach 66% (Wei et al. 2013). However, it is also shown that the efficiency diminishes with increasing temperature differences between the collector plate and the air temperature. Experiments have been carried out in order to describe the rate at which this loss occurs. This rate is estimated at −9.57 $(W \cdot m^{-2} \cdot K^{-1})$, which is estimated from the trend line in Figure 5b (Wei et al. 2013). In order to improve the efficiency of the thermal collector, natural conduction of heat from the absorber plates to the ambient air should be prevented.

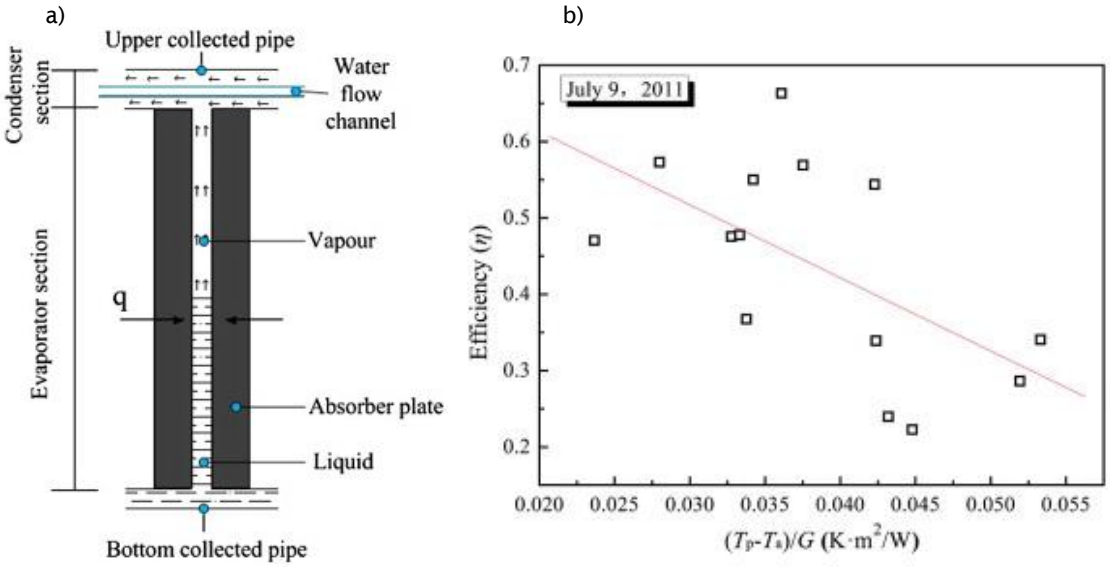

Figure 5: a) Heat transfer inside a solar heat collector pipe. **b)** Collector efficiency versus $(T_p - T_a)/G$ *Source: (Wei et al. 2013)*

2.3 Dry cooler

Various methods of cooling water with the ambient temperature are identified. A widely used method to cool water is the cooling tower, where a warm fluid (usually water) is sprayed upon a fill area and subsequently carried to a collection reservoir (Figure 6a)(Evans 2012). The fill area is made out of sponge-like material where the water may spread out. Some of the fluid evaporates and is blown out of the tower whereas the other part drips out to the collection reservoir. The evaporative process is responsible for the cooling of the fluid. However, for the purpose of this research a wet cooling tower like in Figure 6a is not the best option. First of all the temperature gains in this cooling tower are not very high, which makes the cooling capacity lower(Lucas et al. 2008). Apart from that, at temperatures below 0°C problems may occur with freezing of the cooling fluid. This is unfavorable because at low temperatures, the potential cooling capacity will be highest. A better option might be the dry cooler depicted in Figure 6b. Here the air is forced over a relatively big contact area of piping filled with a fluid called glycol. This fluid has the property that its freezing point is much lower than water. Therefore the dry cooler may operate at lower temperatures and at higher capacities (Evans 2012). Operating capacities for the dry cooler are estimated to be in a range between 8 to 2219 kW, depending on the design and size of the cooler (ThermoKey n.d.).

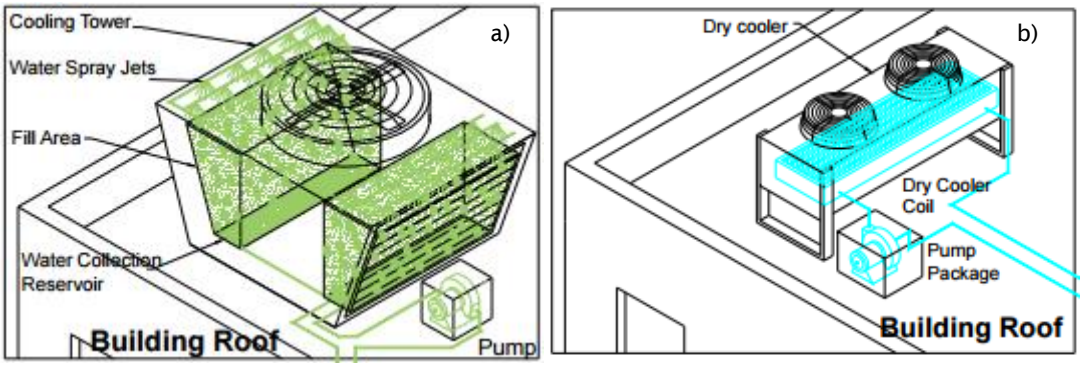

Figure 6: Example of **a)** a cooling tower and **b)** a dry cooler on top of a roof. *Source: (Evans 2012)*

2.4 Heat exchangers

The thermal energy from the storages is carried to the building via a heat exchanger. Heat exchangers are available in varying sizes and designs, each having their own benefits. Most heat exchangers are two-fluid heat exchangers, where two fluids are streaming in close contact and hence may exchange thermal energy. In this study a plate heat exchanger is considered. In a plate heat exchanger, two thin plates are placed on top of each other with a small spacing which forms flow channels. (Kakac et al. 2012) The amount of heat which is exchanged in a heat exchanger can be described as:

$$\boldsymbol{Q_{HE} = \rho_w * C_w * u * \left(T_{HE}^{out} - T_{HE}^{in}\right)} \quad (4)$$

Where the amount of heat which is transported in the heat exchanger $Q_{HE}(J/s)$ is a function of the density of water $\rho_w(kg \cdot m^{-3})$, the heat capacity of water $C_w(J \cdot kg^{-1} \cdot K^{-1})$, the pumping rate through the heat exchanger $u\ (m^3 \cdot s^{-1})$ and the difference of between the temperature coming into and going out of the heat exchanger $(T_{HE}^{out} - T_{HE}^{in})$(Rostampour et al. 2017).

3 Methods

Description of the triplet model, subsurface model and methods of testing the potential of an ATES triplet.

3.1 Triplet model

In order to quantify the fluxes of volume, temperature and energy an analytical model is developed. This model is designed to calculate the interactions between the storages and the building and is henceforth regarded as the triplet model. The triplet model is based on equation (4) and is dictated by the heating and cooling demands from the building. The full expression used in the triplet model can be found in Appendix C.

3.1.1 Heating and cooling demand

How much heating and cooling is demanded from the building is determined by making use of the Heat Degree Days (HDD) method. In literature this method has proven to be a useful and simple method to measure the heat demand during the course of a day (Christenson et al. 2006; De Rosa et al. 2014). The main assumption in the calculation of the HDD is that the demand is linearly related to the difference between the air temperature and a base temperature inside a building. The base temperature represents the desired temperature inside the building, minus the internal heat gains. In this study the ideal temperature inside an office building is stated to be 20˚C and the building is assumed to be occupied by employees or computers producing additional heat gains of 3˚C. So the base temperature for the heat or cold degree days (CDD) is 17˚C and the number of heat degree days per time step is calculated as:

$$\begin{cases} \boldsymbol{HDD_i} & = (\boldsymbol{T_{base}} - \boldsymbol{T^i_{air}}) \cdot \boldsymbol{\Delta t} \quad \boldsymbol{for} \quad \boldsymbol{T_{air} < T_{base}} \\ \boldsymbol{CDD_i} & = (\boldsymbol{T^i_{air}} - \boldsymbol{T_{base}}) \cdot \boldsymbol{\Delta t} \quad \boldsymbol{for} \quad \boldsymbol{T_{air} > T_{base}} \end{cases} \qquad (5)$$

Were $T_{base}(°C)$ indicates the base temperature, $T^i_{air}(°C)$ the ambient air temperature, i represents the i-th time step, $\Delta t(days)$ the length of the time step and $HDD/CDD\ (°C \cdot hour)$ respectively represent the amount of HDD and CDD. To calculate a heating or cooling demand from the HDD or CDD, additional information is required on the use of energy per HDD. Fair estimations on the energy use are supported with research on yearly energy uses in different building sectors for a marine climate in the Netherlands (Meijer et al. 2009). The heating or cooling demand per time step then is:

$$\boldsymbol{f_{demand}} = \frac{\boldsymbol{yearly\ heat\ demand\ (MWh)}}{\sum_{i=1}^{365/\Delta t} \boldsymbol{HDD_i}} \quad \textbf{and} \quad \boldsymbol{Q_{heat,i}(MWh)} = \boldsymbol{HDD_i \cdot f_{demand}} \qquad (6)$$

Where f_{demand} is the fraction of the yearly heat demand, the yearly heating demand is supported by (Meijer et al. 2009) and $Q_{heat,i}$ represents the heat demand in the i-th time step. Note that the cool demand per time step is calculated analogue to the heat demand and that in this study the length of one time step is one hour.

3.1.2 Volumes

With the heating and cooling demands as a driver for the triplet model, the pumping rates are determined by making use of equation (4). A derivation of the pumping rates is given in Figure 7.

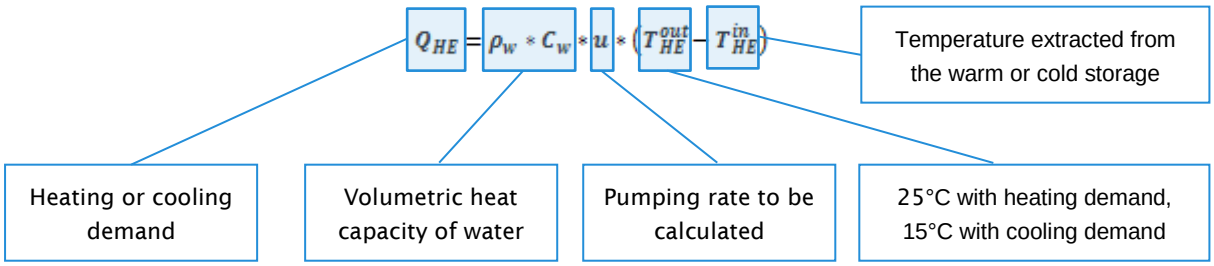

Figure 7: Calculating the pumping rates

Remember that during a period of heat demand, the solar heat collectors can provide heat directly to the building. So during a period of heat demand the volume pumped out of the warm storage is calculated by

making use of the heat demand calculated in equation (6) minus the heat which the solar heat collectors provide. When the pumping rates are known, the hydraulic volumes of the storages are expressed as:

$$V_{WW}^{i} = V_{WW}^{i-1} + dV_{W}^{i-1} \quad (7)$$

Where V_{WW} (m^3) is indicating the hydraulic volume of the warm storage and $dV_W(m^3)$ the pumping rate into the warm well. Note that the hydraulic volumes of the cold and buffer storages are calculated analogue to the warm storage.

3.1.3 Dry cooler & Solar heat collector

The derivation of pumping rates can also be used to calculate the pumped volumes to the dry cooler and the solar heat collectors. The exchanged heat Q_{HE} is in that case equal to the power of the solar heat collector or the dry cooler, like depicted in Figure 8.

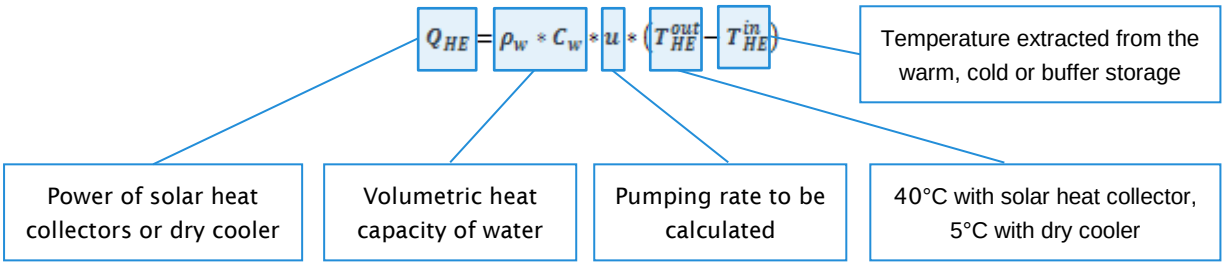

Figure 8: Calculating pumping rates for dry cooler and solar heat collector

The power of the solar heat collectors depends on the amount of energy coming in by solar radiation. The efficiency of converting solar radiation into heat can reach up to 66%, but the efficiency declines with increasing temperature differences between the collector plates and the air temperature (Wei et al. 2013). In this study it is assumed that the plates are the same temperature as the water injected in the warm storage. The efficiency of the dry cooler is based on the assumption that more water can be cooled down with decreasing temperatures. Note that both the power of the dry cooler and the solar heat collectors are design variables, so they can be adjusted according to the need for cooling or heating from the building. The power of the solar heat collectors and the dry cooler are expressed as:

$$P_{pt}^{i} = Q_{rad}^{i} \cdot A \cdot \left(\eta_{pt} - \frac{|T_{aq,w_{in}} - T_{air}^{i}|}{\beta}\right) \quad (8)$$

$$P_{dc}^{i} = \begin{cases} P_{dc,max} & for \quad T_{air} < 0 \\ P_{dc,max}\frac{(T_{aq,c_{in}} - T_{air}^{i})}{T_{aq,c_{in}}} & for \quad 4°C > T_{air} > 0 \\ 0 & for \quad T_{air} > 4°C \end{cases} \quad (9)$$

Where the power of the solar heat collector P_{pt} (MW) is a function of the incoming solar radiation Q_{rad} $(MW \cdot m^{-2})$, the effective area of the solar heat collectors A (m^2), the efficiency of the solar heat collectors $\eta_{pt} = 0.66\,(-)$, the temperature injected into the warm well $T_{aq,w_{in}}$ $(°C)$, the air temperature T_{air} $(°C)$ and the efficiency loss with temperature discrepancy $\beta = 100\,(°C)$. The power of the dry cooler $P_{dc}(MW)$ is a function the maximum dry cooler power $P_{dc,max}(MW)$, the air temperature and the temperature injected into the cold well $T_{aq,c_{in}}$ $(°C)$. Note that the decline in efficiency for the solar heat collectors is not presented analogue to the relation suggested by Wei et al. 2013. However, to prevent negative values of P_{pt} in the triplet model, an alternative form is used which leads to a similar decline in efficiency with increasing temperature differences between the collector plates and the air.

3.1.4 Thermal energy

To prevent inefficient pumping it is important to know how much energy needs to be injected in the cold or warm well before the storage reaches its maximum thermal energy. The heat which the water from the warm or cold storage can respectively release or take up from the space inside the building determines the amount of thermal energy in the storage. This means that the thermal energy in the aquifer storages also depends on the reference temperature to which the water may be cooled down or heated up. The reference temperatures

for the warm, buffer and cold storage respectively are 25˚C, 5˚C and 15˚C. Subsequently, the amount of thermal energy in an aquifer storage is expresses as:

$$E^{i}_{th,WW} = C_w * V^{i-1}_{WW} * |T^{i-1}_{aq,w} - T_{ref,w}| + Q^{i-1}_{w} \quad (10)$$

Where $E_{th,WW}$ (MWh) represents the thermal energy of the warm storage, C_w $(MWh \cdot m^{-3} \cdot °C^{-1})$ the volumetric heat capacity, $V_{WW}(m^3)$ the hydraulic volume of the storage, $T_{aq,w}$ $(°C)$ the average temperature of the warm storage, $T_{ref,W}$ $(°C)$ the reference temperature for the warm storage and Q (MWh) the charge of thermal energy. The charge of thermal energy is expressed as:

$$\begin{cases} Q^{i-1}_{w} = C_w \cdot dV^{i-1}_{W} \cdot |T^{i-1}_{aq,w_{in}} - T_{ref,w}| & for \quad dV_w > 0 \\ Q^{i-1}_{w} = C_w \cdot dV^{i-1}_{W} \cdot |T^{i-1}_{aq,w} - T_{ref,w}| & for \quad dV_w < 0 \end{cases} \quad (11)$$

The charge and thermal energy of the cold and buffer storage are calculated analogue to the warm storage.

3.1.5 Temperatures

The injected temperatures will converge to the ambient groundwater temperature $T_{aq,amb}$ $(°C)$. This process is regarded as the thermal losses. The storage temperatures and the thermal losses can be represented in two ways. The first method is presented in Appendix D, but is unsupported in literature. The second method, henceforth considered as the α-method, is described earlier by (Rostampour et al. 2016) and yields - especially for lower storage temperatures - better results. In the α-method a loss term α $(-)$ is introduced which represents the losses of the volume averaged storage temperature $T_{aq,w}(°C)$ in the subsurface:

$$T^{i}_{aq,w} = \frac{V^{i-1}_{WW} \cdot T^{i-1}_{aq,w}}{V^{i-1}_{WW} + dV^{i-1}_{W_{in}}} + \frac{dV^{i-1}_{W_{in}} \cdot T^{i-1}_{aq,w_{in}}}{V^{i-1}_{WW} + dV^{i-1}_{W_{in}}} - \alpha \cdot \frac{(T^{i-1}_{aq,w} - T_{aq,amb})}{V^{i-1}_{WW} + dV^{i-1}_{W_{in}}} \quad (12)$$

The first term represents the volume averaged temperature of the water that was already pumped into the storage in previous time steps. The second term represents the volume averaged temperature of the water that is pumped into the storage. Finally the third term represents the loss term α which causes the storage temperature to converge to the ambient groundwater temperature $T_{aq,amb}$ $(°C)$. So when the storage volume decreases or the temperature difference between the storage and the ambient groundwater is bigger, the storage temperature converges more quickly towards the ambient groundwater temperature. Note that the average temperatures of the cold and buffer storages are calculated analogue to the warm storage.

3.1.5.1 Loss term

The loss term α is previously described by (Rostampour et al. 2016) as:

$$\alpha = a * \left(\frac{H}{D}\right)^2 + b * \left(\frac{H}{D}\right) + c \quad (13)$$

With a $(-)$, b $(-)$ and c $(-)$ respectively estimated at $0.45, 0.5$ and 0.33, H (m) is the filter screen length and D (m) the distance between the storages. Previous studies suggest that the spacing between the storages should be three times the thermal radius R_{th} (Bloemendal et al. 2013; Sommer et al. 2015), where the thermal radius is expressed as:

$$R_{th} = \sqrt{c_w * \frac{V}{c_d * \pi * H}} \quad (14)$$

Here c_w $(J \cdot m^{-3} \cdot K^{-1})$ is the heat capacity of water, c_d $(J \cdot m^{-3} \cdot K^{-1})$ the heat capacity of the aquifer (sand and water combined) and V (m^3) is the hydraulic volume of the storage.

3.1.6 Cut-off temperature

Below 30˚C it is not possible to provide effective heating with a floor heating system (Bloemendal et al. 2013) and other (non-sustainable) heat sources are necessary to provide in a heating demand. Therefore, a cut-off temperature of 30˚C is defined for the warm storage. When the temperature of the warm storage falls below the cut-off temperature, the warm storage is considered empty and the volume and temperature of the warm storage are reset.

3.2 Subsurface model

In order to study the thermal losses in the subsurface in more detail, the subsurface model is developed. The processes of heat transport in the subsurface are simulated by using a finite difference model called SEAWAT v4 to solve the Richard's equation for flow and transport (Langevin et al. 2008). SEAWAT couples the USGS MODFLOW2000 code for groundwater flow simulation to the species transport simulation program called MT3DMS, which makes it possible to visualize the effects of varying density on the groundwater flow. The temperature of the groundwater is visualized as the concentration of a species, where the density is a linear function of the temperature suggested by (Thorne et al. 2006):

$$\boldsymbol{\rho = \rho_0 - 0.375 \cdot T} \qquad (15)$$

Here, ρ is the variable density, ρ_0 ($^{kg}/_{m^3}$) is the reference density ($= 1000\ kg/m^3$) and T ($°C$) the temperature of the groundwater. Similarly the effects of temperature on the viscosity of the groundwater are simulated by implying a relation between temperature and viscosity, suggested by (Langevin et al. 2008):

$$\boldsymbol{\mu(T) = A_1 \cdot A_2^{\frac{A_3}{T+A_4}}} \qquad (16)$$

Where μ is the dynamic viscosity, $T(°C)$ the groundwater temperature and the constants A_n *(-)* are specified by the user. In this study the constants are listed in Table 2, based on previous work by (Langevin et al. 2008).

3.2.1 Subsurface model setup

The following six assumptions are made regarding the setup of the subsurface model:

- The three storages are assumed to be cylindrical shaped and situated in a completely confined aquifer like in Figure 9.
- The spatial planning of the storages is intuitively chosen to be a triangle, so that the storages take the smallest space in the subsurface.
- The filter length is chosen with respect to the storage volume of the warm storage, so that the ratio of area divided by volume (A/V ratio) is the smallest for the warm storage and the thermal losses are minimized (Bloemendal et al. 2016).
- Fine sanded aquifers, situated at a depth of 100m below the surface, are used for storing the water. This means that the background flow and the impact of the atmosphere are negligible. In addition, the hydraulic conductivities will be lower with respect to coarse sanded aquifers.
- In order to simulate the potential interaction between the storages, the model is setup to be three-dimensional. The discretization of the subsurface space is setup in such a way that the smallest cells are near the well (diameter =1m), and the biggest cells are at the outer boundaries ($\Delta x = 50m$).
- The outer boundaries of the model are assigned constant head and temperature. Therefore the aquitards are modeled relatively thick (20m) compared to typical aquitards (<3m), so that there is no active cooling or warming from the outer boundaries.

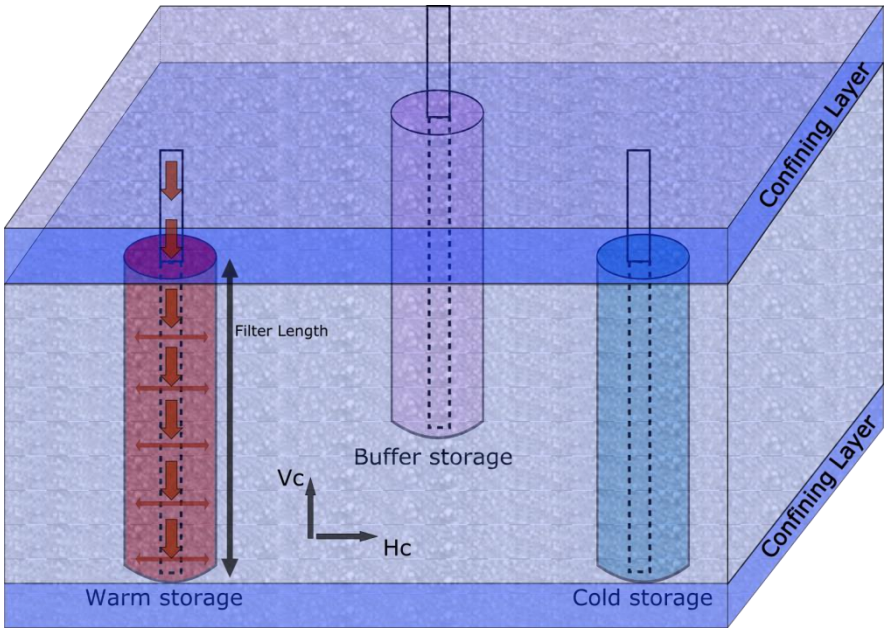

Figure 9: Conceptual visualization of the subsurface model. Vc and Hc indicate the vertical and horizontal conductivities.

3.3 Communication between triplet & subsurface model

The triplet model calculates the pumping rates from the storages with the heating and cooling demands as a driver, whereas the subsurface model calculates the heat transfer processes in the subsurface with the pumping rates as a driver. Therefore the triplet and subsurface model are required to communicate outputs. The communication between the subsurface and triplet model can be realized in three different ways.

3.3.1 Using only triplet model

The first option (Figure 10a) is to only use the triplet model, so that the thermal losses in the subsurface are presented by the loss term described in section 3.1.5.1. Because the triplet model is built up of analytic relations, this method is the fastest in terms of computational time. However, this method lacks the ability to present the subsurface processes in detail and is henceforth regarded as calculation method 1 (CM1).

3.3.2 Triplet output to subsurface input

In the second option (Figure 10b) the pumping rates are calculated by making use of the triplet model and the temperature representation as in equation (12). To obtain more detail regarding the subsurface processes, the pumping rates are exported to the subsurface model which takes the pumping rates as an input. This option improves the level of detail regarding the processes in the aquifer, but is more computational intensive compared to using only the triplet model. From now this method is called calculation method 2 (CM2).

3.3.3 Hourly communication between triplet and subsurface model

As observed from Figure 7, the pumping rates and storage temperatures are related. Hence a third option (Figure 10c) is introduced where the pumping rates are exported from the triplet model to the subsurface model on an hourly basis. Subsequently the initial conditions of the triplet model and the subsurface model are updated each 24 hours by making use of the subsurface model outputs. Therefore this option shows the pumping rates and storage temperatures in highest detail, but also incorporates the longest run times. Option three will henceforth be denoted as calculation method 3 (CM3).

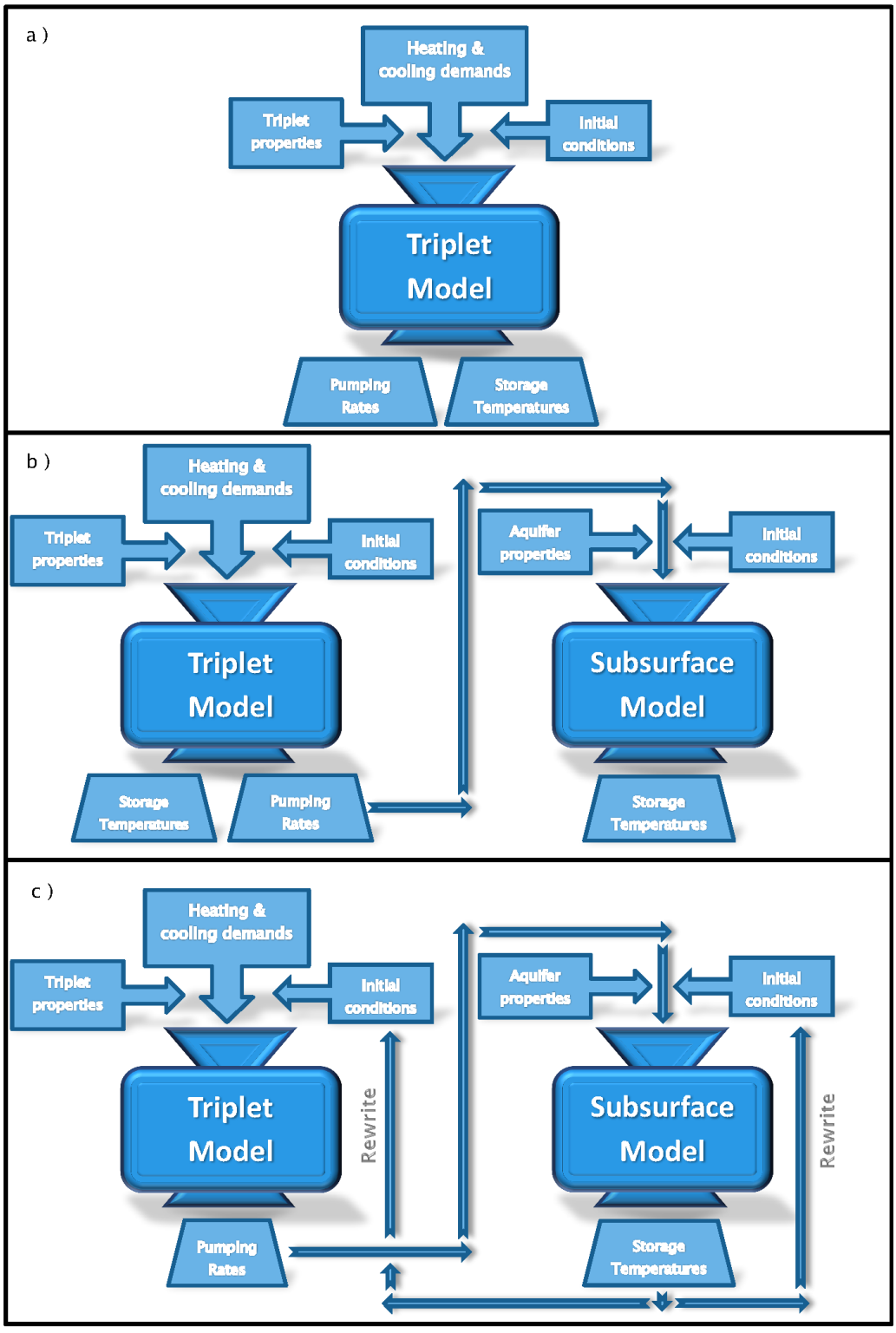

Figure 10: Schematic visualization of model communication. **a)** Inputs and outputs when only using the triplet model. **b)** Inputs and outputs by making use of the triplet and subsurface models in sequence. **c)** Inputs and outputs when using the triplet and subsurface models to communicate on an hourly basis

3.4 Assessment framework

First the metrics to measure the performance of the ATES triplet are described, then the conditions for the feasibility are determined and finally the sensitivity analyses are described.

3.4.1 Thermal Performance

The thermal energy pumped into and out of the storages is registered by using equation (10). The ratio between the injected and extracted thermal energy per recover cycle is expressed as the thermal recovery:

$$\epsilon = \frac{E^{out}_{therm}}{E^{in}_{therm}} \qquad (17)$$

Where $E^{out/in}_{therm}\ (MWh)$ is the thermal energy pumped in or out the aquifer and a recovery cycle is regarded as one year from the beginning of spring to the end of winter. In literature the thermal recovery is used to analyze the performance of ATES systems, e.g. (van Lopik et al. 2016; Sommer et al. 2015). However, there are also scenarios where energy is injected in the first recovery cycle but retrieved in the second due to varying weather conditions. Therefore the thermal recovery will not give representative measures for the performance of each recovery cycle and the thermal efficiency is considered instead. The thermal efficiency is formerly described as the ratio between thermal efficiency and the thermal efficiency if there would be no losses (Sommer et al. 2015).

$$\eta = \frac{\epsilon}{\epsilon_{no\ loss}} = \left(\frac{E^{out}_{therm}}{E^{in}_{therm}}\right) / \left(\frac{E^{out}_{therm,no\ loss}}{E^{in}_{therm,no\ loss}}\right) = \frac{\sum_{i=1}^{N} C_w \cdot u^i_{out} \cdot \left|T^i_{extracted} - T_{ref}\right| \Delta t^i}{\sum_{i=1}^{N} C_w \cdot u^i_{out} \cdot \left|T^i_{injected} - T_{ref}\right| \Delta t^i} \qquad (18)$$

Here $\eta\ (-)$ is the thermal efficiency, $C_w (MWh \cdot m^{-3} \cdot {}^{\circ}C^{-1})$ is the volumetric heat capacity of the aquifer, $dV_{out} (m^3/s)$ is the pumping rate out of the storage, $T_{extracted}, T_{injected}\ and\ T_{ref}\ ({}^{\circ}C)$ respectively are the temperatures of the extracted water, the injected water and the reference temperature, i denotes the time step and $\Delta t\ (s)$ the length of the time step.

3.4.2 Environmental & Economic performance

In order to compare the ATES triplet with respect to conventional space heating and an ATES doublet, the environmental performance will be considered. This will be measured by the amount of energy/gas use and emissions of CO_2. As explained in section 3.1.1, research done by (Meijer et al. 2009) is used to estimate the heating and cooling demands from the building which are henceforth denoted as $E^j_{heat/cool}\ (MWh)$, where j indicates the recovery cycle. The parameters used for the environmental performance are listed in Table 1.

Table 1: Parameters used in environmental & economic analysis

	Parameter	Symbol	Unit	Value
Constants	Coefficient of performance cooling machine	COP_c	-	3[1]
	Coefficient of performance heat pump	COP_{HP}	-	4[1]
	Efficiency pump	η_{pump}	-	0.25[1]
	Efficiency gas boiler	η_B	-	0.85[1]
	Emission factor electricity	c_e	$(kg\ CO_2 \cdot MWh^{-1})$	460[2]
	Emission factor gas	c_g	$(kg\ CO_2 \cdot MWh^{-1})$	277[2]
	Electricity price	f_e	$€ \cdot MWh^{-1}$	102[2]
	Gas price	f_g	$€ \cdot MWh^{-1}$	32.3[2]
	Required pressure increase for groundwater pumps	ΔP	$MWh \cdot m^{-3}$	$4.08 * 10^{-5}$ [2]

[1](Bloemendal et al. 2017)

[2](Sommer et al. 2015)

3.4.2.1 Energy use

Following previous work (Sommer et al. 2015; Bloemendal et al. 2017), the electricity use of the energy systems $E\ (MWh)$ per recovery cycle j are:

$$\begin{cases} E^j_{conventional} = \frac{E^j_{cool}}{COP_c} \\ E^j_{doublet} = \frac{E^j_{heat}}{COP_{HP}-1} + \int dV^j \cdot \frac{\Delta P}{\eta_{pump}} \\ E^j_{triplet} = \int dV^j \cdot \frac{\Delta P}{\eta_{pump}} \end{cases} \quad (19)$$

Where η_b is the efficiency of the boiler, COP_c is the coefficient of performance for the chiller which drives the cooling in a conventional system, $\int dV^j\ (m^3)$ is the total volume pumped in and out the aquifer for all storages, $\Delta P(MWh/m^3)$ is the hydraulic resistance, η_{pump} is the pumping efficiency and COP_{HP} is the coefficient of performance for the heat pump in a doublet system. The required pressure increase is typically 15 mwc; 5 for the discharge head and 10 to overcome the resistance in the piping and the heat exchangers. It is assumed that an ATES doublet provides free cooling by using ambient groundwater temperatures.

3.4.2.2 Gas use

For the ATES triplet as well as the doublet, there is no gas use. For the conventional system however, the heating demand is supplied by a gas boiler. This boiler is assumed to have an efficiency η_B and its gas use $G\ (MWh)$ is described as:

$$G^j_{conventional} = E^j_{heat} \cdot \eta_B^{-1} \quad (20)$$

3.4.2.3 CO_2 emissions and operational costs

The CO_2 emissions are calculated by assuming a constant emission rate for electricity and gas use c_e and c_g $(kg\ CO_2 \cdot MWh^{-1})$. The total amount of emitted CO_2, $C^j\ (kg\ CO_2)$ can subsequently be expressed as:

$$\begin{cases} C^j_{conventional} = E^j_{conventional} \cdot c_e + G^j_{conventional} \cdot c_g \\ C^j_{doublet} = E^j_{doublet} \cdot c_e \\ C^j_{triplet} = E^j_{triplet} \cdot c_e \end{cases} \quad (21)$$

The operational costs are calculated analogue to this method, by making use of energy cost factors f_e and f_g $(€ \cdot MWh^{-1})$ instead of the emission factors c_e and c_g.

3.4.3 Economic feasibility

To provide a robust perspective on the economic feasibility of an ATES triplet, the operational costs provide a too narrow view. A more supported approach is suggested regarding the economic benefits of the ATES triplet with respect to a conventional system and an ATES doublet. The Total Costs of Ownership (TCO) consider the installation, maintenance and developing costs of the systems over a predefined period of ownership including the reduction in value of each element (Martin Bloemendal et al. 2016). The TCO analysis provided in this study makes use of the assumptions shown in Appendix A. These assumptions are based on previous TCO analyses on ATES doublets by the KWR watercycle research institute (Martin Bloemendal et al. 2016; Jan Hofman et al. 2015). The ATES triplet is stated to be economically feasible when the TCO are less compared to an ATES doublet or conventional systems.

3.4.4 Technical feasibility

The technical feasibility is translated into two conditions to which the ATES triplet must comply. The first condition is that the solar heat collectors and the dry coolers must fit on the roof of the building. Because the dry cooler can be placed under the solar heat collectors and the maximum roof area is equal to the GSA, this condition can be reduced to the statement that the area of solar heat collectors cannot be larger than the GSA. The second conditions requires the warm and the cold storage to provide in the heating and cooling demands. In temperate climates like in the Netherlands, effective cooling can also be realized by using ambient groundwater temperatures. Therefore the second condition can be reduced to the statement that the temperature of the warm storage is required to stay above the cut-off temperature of 30˚C.

3.4.5 Sensitivity Analyses

In order to make a thorough analyses of the ATES triplet feasibility under different conditions, this study investigates the effect of six parameters on the performance of the ATES triplet:

- Building sizes & storage volumes
- Injection temperatures
- Filter lengths
- Hydraulic conductivities
- Density effects
- Weather conditions

All scenarios aim to gain insight in the behavior of the system under different conditions and subsequently answer the research questions in section 1.1. Note that in all scenarios (except for varying the weather conditions) the performance of the warm storage is specifically investigated because a temperate climate is considered. This means that the main challenge will be storing warm instead of cold water. First of all because the temperature differences are higher with respect to the ambient groundwater temperatures and secondly because the weather conditions demand for more heating instead of cooling. Hence the performance of the ATES triplet will mainly be dictated by the performance of the warm storage.

3.4.5.1 Reference scenario

First, a reference scenario is introduced, which puts the results of the sensitivity analysis into perspective. For this reference scenario an example building is used which properties (listed in Table 2) are similar to the 3mE building on the TU Delft campus (Figure 11a). In Figure 11b the location of the wells are indicated, as well as the metrics to estimate the roof area. The aquifer properties are assigned as typical fine-sanded aquifer properties and are also listed in Table 2. The results are calculated by making use of CM2 with a 5 year (2011 to 2016) KNMI dataset (KNMI n.d.), containing hourly values of air temperature at the canopy layer and incoming solar radiation at the surface as an input. Note that in order to start with a cooling demand, the system has to start up in spring (ref. section 2.1.6) and the data from the first winter months of 2011 are appended after the last data of 2016.

Table 2: Properties of reference scenario.

	Input Parameter	Value	Units	Comments
Building properties	Building type	Office	-	Building property[3]
	Gross surface area	40,000	m^2	Assigned
	Roof Area	8000	m^2	Assigned
	Hours in use	70	Hours/week	Assigned
	Power dry cooler	1360	kW	Assigned
	Area solar heat panels	6,400	m^2	Assigned
	Heating demand per m^2	35.6	$kWh \cdot m^{-2}$	From literature[2]
	Cooling demand per m^2	9	$kWh \cdot m^{-2}$	From literature[2]
Grid properties	Minimum cell size	1	m	Assigned
	Maximum cell size	50	m	Assigned
	Steps between min and max cell size	20	-	Assigned
	Number of aquifer layers	10	-	Assigned
	Number of aquitards layers	2 times 4 layers	-	Assigned
	Layer thickness (ΔZ)	5	m	Assigned
	Grid extents	[0,500,0,500]	m	Assigned
Aquifer properties	Horizontal conductivity K_{ho}	10	m/day	Assigned
	Vertical conductivity K_{v0}	2	m/day	Assigned
	Specific storage S_s	$1 \cdot 10^{-5}$	m	
	Porosity (θ)	0.35	-	Assigned
	Longitudinal dispersivity (α_L)	1	m	Assigned
	Transversal dispersivity (α_T)	0.1	m	Assigned
	Thermal conductivity solid (k_{Tsolid})	3.59	$W \cdot m^{-2} \cdot °C^{-1}$	Approximate value for calcite
	Density of solid (ρ_s)	2,710	$kg \cdot m^{-3}$	Approximate value for calcite
	Bulk density (ρ_b)	1,762	$kg \cdot m^{-3}$	Calculated
	Bulk thermal diffusivity ($D_{m_{temp}}$)	0.1503	$m^2 \cdot d^{-1}$	From literature[1]
Fluid properties	Heat capacity of water	4,183	$J \cdot kg^{-1} \cdot °C^{-1}$	Value for water
	Thermal conductivity of water ($k_{T_{fluid}}$)	0.61	$W \cdot m^{-1} \cdot °C^{-1}$	
	Distribution coefficient for temperature ($K_{d_{temp}}$)	$2 \cdot 10^{-4}$	$m^3 \cdot kg^{-1}$	From literature
	Reference density ρ_0	1000	$kg \cdot m^{-3}$	Assigned
	Temperature change $\delta\rho/\delta T$	-0.375	$kg \cdot m^{-3} \cdot °C^{-1}$	From literature[1]
	Reference temperature (T_0)	0	°C	Assigned
	Constants used for viscosity-temperature relation:			
	A_1	$2.394 \cdot 10^{-5}$	-	From literature[1]
	A_2	10	-	From literature[1]
	A_3	248.37	-	From literature[1]
	A_4	133.15	-	From literature[1]
Other	Temperature in warm well	40	°C	Assigned
	Temperature in cold well	5	°C	Assigned
	Filter Length	55	m	Assigned
	Simulation period	5	Years	Assigned
	Time step length triplet model	1	Hours	Assigned
	Time step length subsurface model	1	Days	Assigned

1 (Langevin et al. 2008)
2 (Meijer et al. 2009)
3 (Delft 2013)

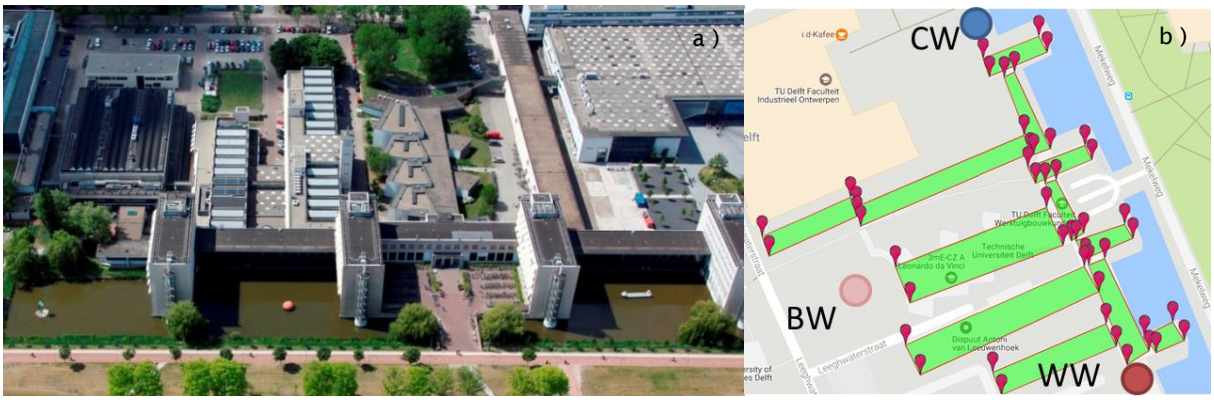

Figure 11: TU Delft campus **a):** The faculty of Mechanical, Maritime and Materials Engineering (3mE, 1953) *Source: (Delft 2013)* **b):** Estimated roof area with Google maps distance tool and spatial planning of the wells.

3.4.5.2 Building sizes & storage volumes

In order to study the effect of different storage volumes on the triplet feasibility, the building sizes are varied. The building sizes are directly related to the demand for heating and cooling and hence also to the required size of the storage volumes. The results are calculated using CM2 and the GSA is increased exponentially as:

$$Gross\ surface\ area \quad = \quad 40.000m^2 \cdot 2^x, \quad where \quad x\ \epsilon[0,1,2,3]$$

The filter lengths, the area of solar heat cells and the power of the dry cooler are scaled proportionally to the GSA. The filter lengths are chosen so that the A/V ratio (regarding the warm storage) is minimized. The filter lengths with the minimized A/V ratio are then required to be in a range of 1 to 2.5 of the filter length divided by the thermal radius (L/R_{th} ratio), which is suggested in previous work (Bloemendal et al. 2016). However, a more suitable filter length can reduce the thermal losses and hence lead to a reduced storage volume, which makes the estimation of the ideal filter length a time-consuming iterative process. Therefore the filter lengths are estimated by making use of the storage volume calculated with CM1, the relation sketched in Figure 12 and a reference filter length of 55m.

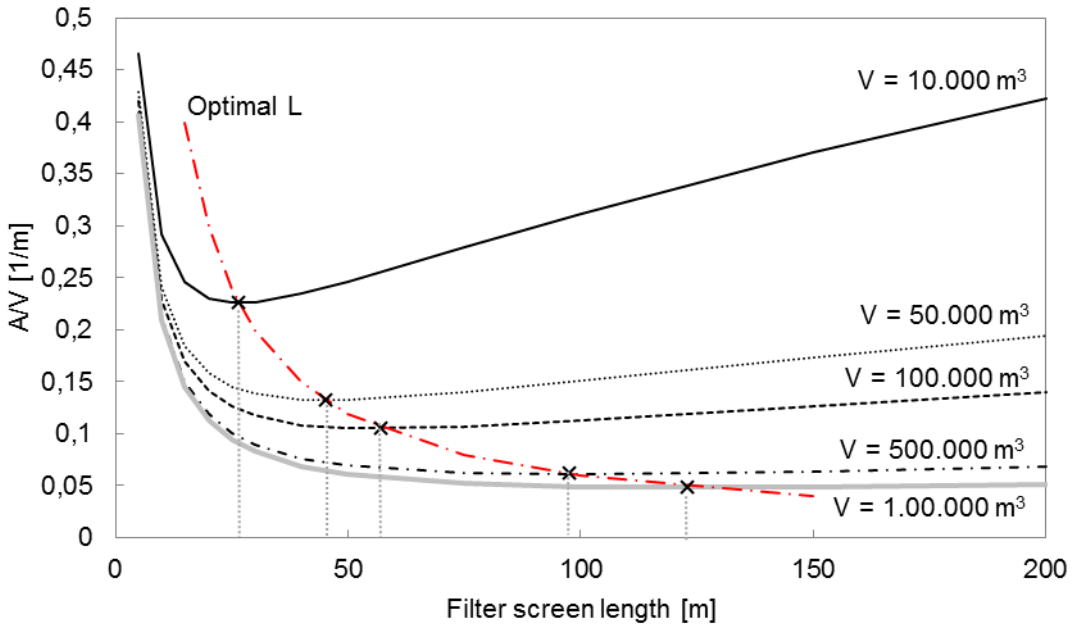

Figure 12: Optimal filter lengths (L) for different storage volumes. *Source: (Bloemendal et al. 2016)*

3.4.5.3 Injection temperatures

The injection temperatures are varied in order to study the effects on the performance of higher and lower injection temperatures into the warm well. In order to keep away from the problems occurring with HT storage, and from the cut-off temperature the injection temperatures are chosen close to 40˚C. The results are calculated using CM2.

$$T_{inj} = [35,40,45,50]^{\circ}\mathrm{C}$$

3.4.5.4 Filter lengths

The filter lengths are varied in order to study the effects of the A/V ratio. One filter length is causing a 'pancake-shaped' cylinder, whereas the other causes a thin pipe profile. Both profiles will cause the A/V ratio to raise, as is shown Figure 12. Hence the following scenarios are calculated by making use of CM2:

$$L = [25,55,120]m$$

3.4.5.5 Density effects

With higher injection temperatures, density driven flow or buoyancy will influence the recovery of the warm storage. To what extent this property is affecting the thermal losses and hence the performance of the triplet system is presented here. Previous work has shown that high temperature (~70˚C) storages greatly influence the thermal recovery efficiency due to enhanced free convection by buoyancy and decreased viscosity at higher temperatures (van Lopik et al. 2016). The effects of temperature dependent viscosity and density driven flow and are investigated by making use of the SEAWAT density package. One scenario is calculated with this package and one without. Both scenarios are calculated using CM2.

3.4.5.6 Hydraulic conductivities

The hydraulic conductivities are varied to study the potential of an ATES triplet with respect to different aquifer compositions. In this study the anisotropy (H_c/V_c) is kept constant at 5, so when the vertical conductivity is increased, the horizontal conductivity is increased proportional. The following vertical conductivities are considered by making use of CM2:

$$V_C = [2,5,10]m/day$$

3.4.5.7 Climatologic conditions

Finally a sensitivity analysis is applied on the climatologic conditions. The results are calculated by making use of CM1 because of two reasons. Firstly, with different climates the subsurface properties will also vary and the assumptions regarding the aquifer properties in Table 2 will not be valid anymore. Secondly, a lot of runs are needed in order to determine the minimum requirements regarding the solar heat collectors and the dry cooler before the ATES triplet is technically feasible. Therefore a short runtime is required, which can be realized by making use of CM1. The climate sets which are used to simulate the different weather conditions are visualized in Figure 13. The map shows the potential of ATES doublet systems, which is previously investigated by (Bloemendal et al. 2015).

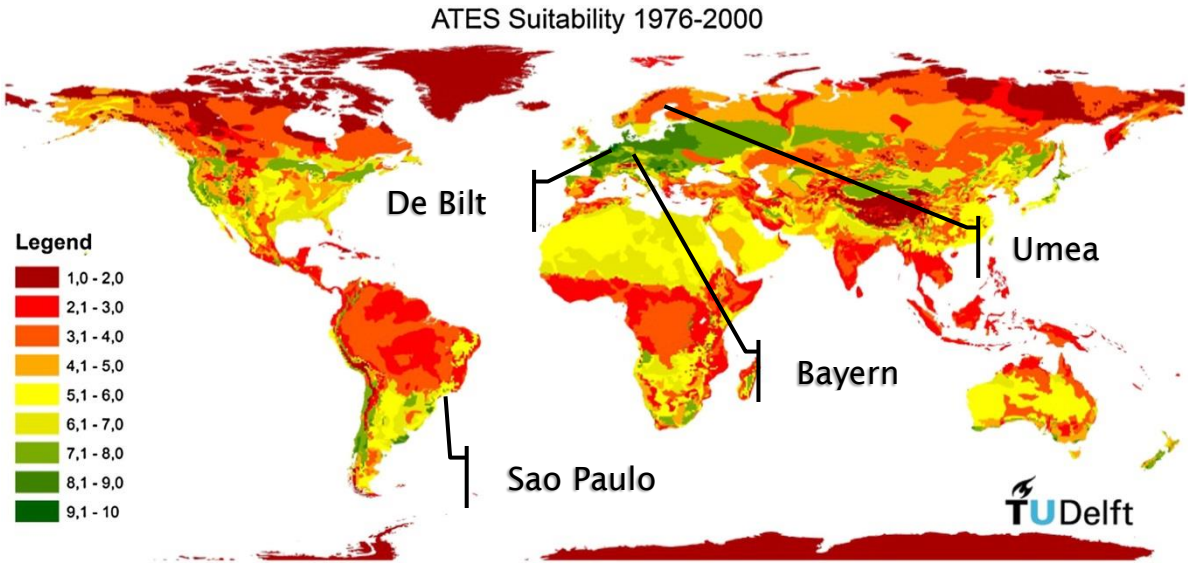

Figure 13: Potential of ATES systems worldwide *(Bloemendal et al. 2015).* The location of the different climate sets which are used are shown with the black labels.

Apart from the dataset of De Bilt, described in section 3.4.5.1, three other datasets are used. First, consider the dataset from Bayern, which yields extremer temperatures but at a comparable yearly average temperature to the De Bilt set. The Bayern dataset contains 4 years of hourly and 10-minute interval based data over a period of 4 years (2012 - 2016). The data is gathered from two weather stations situated in the south of Bavaria (Germany) (Umwelt 2013). Secondly a year of temperature and radiation data is obtained from a station in São Paulo(INMET 2017). This station is situated closer to the equator and is considered as a humid subtropical climate, which is chosen to represent warmer weather conditions. Finally, a dataset from Umea (Sweden) is obtained in order to represent colder weather conditions(SMHI 2017).

In section 3.1.1 the average yearly heat demand is used to calculate hourly heating and cooling demands. In the Netherlands this data is investigated by (Meijer et al. 2009) for buildings situated in the Dutch climate, but this is not representative for the other datasets. Hence the yearly demands for heating and cooling are scaled by making use of the spread in yearly temperatures and the shift in average temperature as:

$$\boldsymbol{demands}\begin{cases} \boldsymbol{CD_{NL}} \cdot \sqrt{\frac{\sigma^2(T_{air}^{sc_x})}{\sigma^2(T_{air}^{NL})}} \cdot \frac{\bar{T}_{air}^{sc_x}}{\bar{T}_{air}^{NL}} = \boldsymbol{CD_{sc_x}} \\ \boldsymbol{HD_{NL}} \cdot \sqrt{\frac{\sigma^2(T_{air}^{sc_x})}{\sigma^2(T_{air}^{NL})}} \cdot \frac{\bar{T}_{air}^{NL}}{\bar{T}_{air}^{sc_x}} = \boldsymbol{HD_{sc_x}} \end{cases} \quad (22)$$

Where CD_{NL} is the average yearly cool demand for the reference scenario in the Netherlands, σ^2 is the variance in the temperature dataset and $\bar{T}_{air}^{sc_x}$ represents the yearly average temperature for an alternative climate scenario x. The first term is based on the assumption that with extremer temperatures the demand will rise, whereas the latter term is based on the assumption that a shift in yearly average temperatures will cause a shift in heating and cooling demands.

3.4.6 Test case

A test case is introduced, based on the properties of the 3mE building in Figure 11, to test the conditions for the technical and economic feasibility. In order to present the results in highest detail, the results will be calculated by making use of CM3. The building properties are listed online (Delft 2013) and the heating and cooling demands are calculated by making use of the data from (Meijer et al. 2009). The local aquifer properties and the suitability for HT-ATES systems at this location is considered in (Hacking 2017). In this work a suggestion is made for the most suitable aquifer regarding high temperature storage. Hence the Maassluis formation is considered as the aquifer to which the water will be injected. This aquifer is estimated to yield horizontal conductivities of $10 \leq H_c \leq 100$ m/day and very low vertical conductivities of $0.001 \leq V_c \leq 1\, m/day$. For the test case V_c is assigned to be $1\, m/day$ with an anisotropy of 10. The parameters which differ from Table 2 are listed in Table 3.

Table 3: Properties of test case

	Input parameter	Value	Units	Comments
Properties	Building type	University	-	Building property[2]
	Gross surface area	46,120	m^2	Building property[2]
	Roof Area	9605	m^2	Estimated from Google maps
	Area solar heat panels	= Roof Area	m^2	Assigned
	Heating demand per m^2	34.2	$kWh \cdot m^{-2}$	From literature[2]
	Cooling demand per m^2	10.1	$kWh \cdot m^{-2}$	From literature[2]
	Horizontal conductivity K_{ho}	10	m/day	From literature[3]
	Vertical conductivity K_{v0}	1	m/day	From literature[3]

1(Meijer et al. 2009)
2(Delft 2013)
3(Hacking 2017)

4 Results

The results of the sensitivity analysis and the test case.

4.1 Sensitivity analyses

The performance of the ATES triplet is measured by presenting the thermal efficiency of the warm storage. The results of the sensitivity analyses are presented in the following sections.

4.1.1 Building sizes

First of all the considered building sizes lead to the following storage volumes and filter length, visualized in Table 4. The storage volume is rounded to the nearest 10.000m^3, the filter length is estimated within a 5m margin.

Table 4: GSA's and corresponding storage volumes and filter lengths

	GSA	Storage Volume	Filter length	Comments
Values	40.000m^2	140.000m^3	55m	Reference scenario
	80.000m^2	270.000m^3	65m	Estimated from Figure 12
	160.000m^2	520.000m^3	95m	Estimated from Figure 12
	320.000m^2	1.010.000m^3	120m	Estimated from Figure 12

The thermal efficiencies for the different building sizes are visualized over the 5 recovery cycles in Figure 15. It is observed that the thermal efficiencies are improving with increasing GSA. In addition, the thermal efficiencies are also improving over the recovery cycles. The increase in thermal efficiency is most pronounced in the third cycle, whereas the increase in the last two cycles is less pronounced or not present at all. The reason for the increased thermal efficiency in the third recovery cycle can be explained by the weather variability. When a mild winter is situated between two more severe winters the drop in temperature is limited. If the temperature drop is limited, there will be less thermal losses and the thermal efficiency is increased.

Whereas the largest buildings shows an improvement of 58% in thermal efficiency with respect to the reference scenario in the first recovery cycle, in the last recovery cycles this improvement is only 11%. This can be explained by the fact that the confining layer is warmed up after a few cycles. This causes the losses at the cap and bottom to be limited and restricts the losses to the circumference. When the cap and bottom are not affecting the thermal losses, the thermal losses are further reduced by minimizing the filter length.

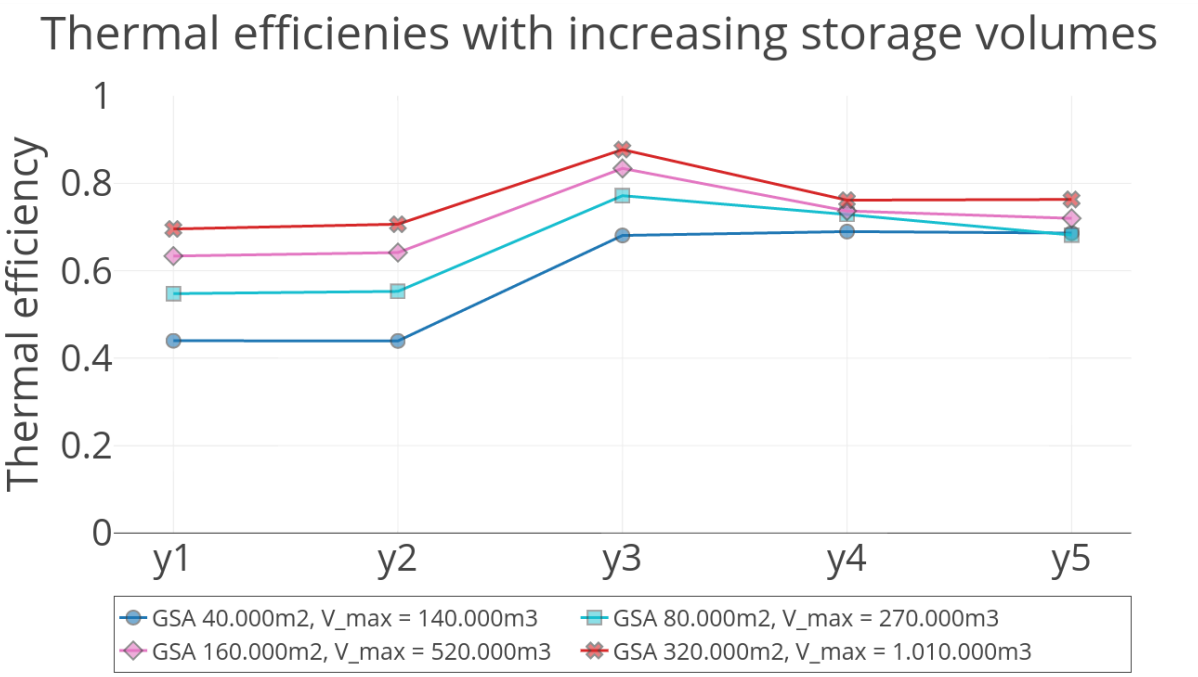

Figure 14: Thermal efficiencies with increasing gross surface area (~ storage volumes) for each recovery cycle (y1,y2,...,y5).

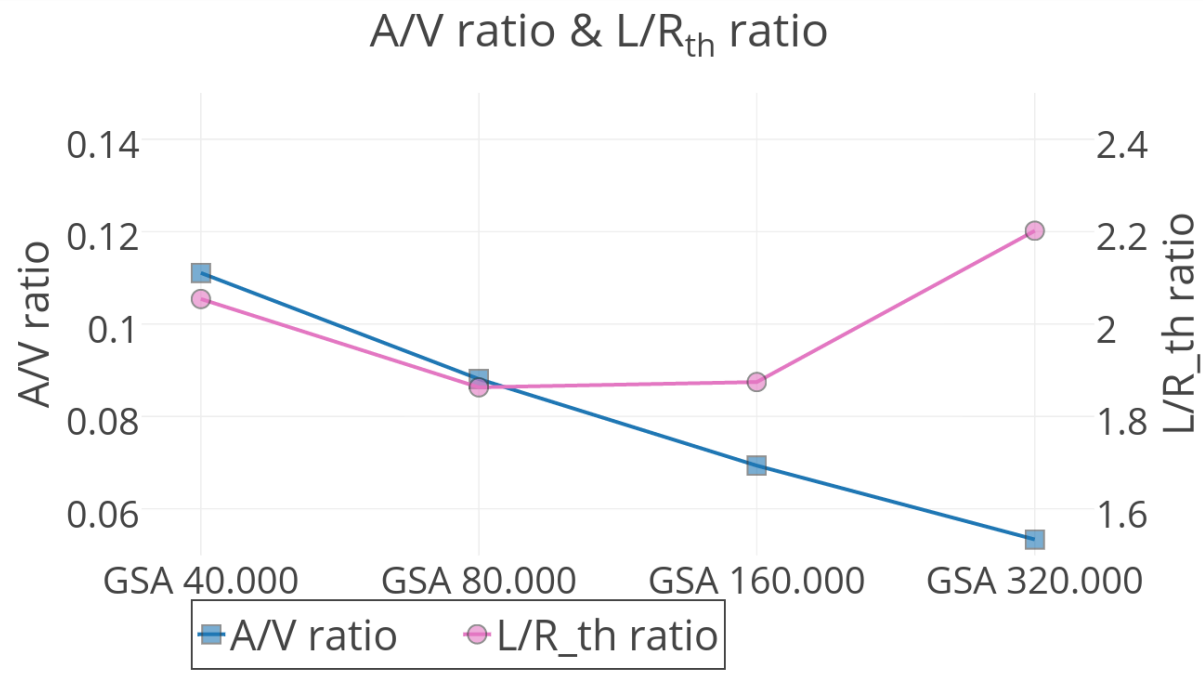

Figure 15: A/V ratio and L/R_{th} ratio for the considered GSA's (~storage volumes).

The increased thermal efficiency with increasing storage volumes can also be explained by looking at the corresponding A/V ratios depicted in Figure 15. Optimal filter lengths are chosen for each storage volume, so the shape of the cylindrical storage stays the same. Therefore, the A/V ratio decreases as the storage volumes increase and the thermal losses occurring at the surface are smaller for bigger volumes. Apart from that, all L/R_{th} ratios are in a range between 1 and 2.5, supporting the estimations of the filter lengths in Table 4 from Figure 12.

4.1.2 Injection temperatures

The impact of varying injection temperatures on the temperature losses are represented in Figure 16, where the temperature at the warm well is shown with respect to V_{out}/V_{in} for each recovery cycle. The fraction V_{out}/V_{in} represents the fraction of volume pumped in the warm storage divided by the volume pumped out of the warm storage in that recovery cycle. It is observed that the temperature decrease is steeper with higher injection temperatures. This is firstly due to the larger temperature difference compared to the ambient groundwater. Secondly, the warm storage requires less storage volume with higher storage temperatures, causing the A/V ratio to increase with increasing storage temperatures. Note that the thermal efficiency increases with lower temperatures than 40˚C, but the cut-off temperature of 30 ˚C is earlier reached (Figure 16d). Therefore a trade-off can be identified between the thermal efficiency and the volume fraction at which the cut-off temperature is reached.

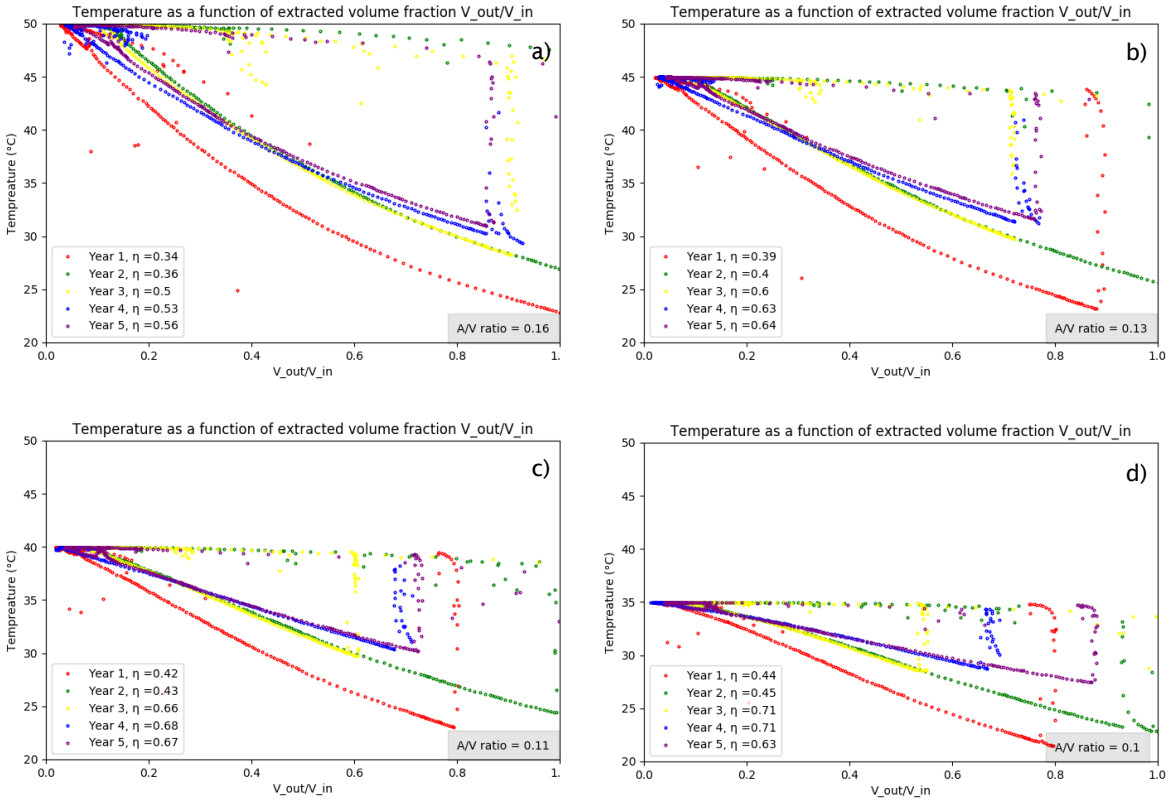

Figure 16: Warm storage temperatures as a function of the ratio between injected and extracted volume. The colors indicate the recovery cycle, the A/V ratio is presented in the bottom right corner of each graph and η is the thermal efficiency. **a)** T_{inj} = 50˚C, **b)** T_{inj} = 45˚C, **c)** T_{inj} = 40˚C, **d)** T_{inj} = 35˚C

4.1.3 Filter Length

The effects of the two alternative filter lengths for a building with a GSA of 40.000m^2 on the thermal efficiency of the warm storage are shown in Figure 17.

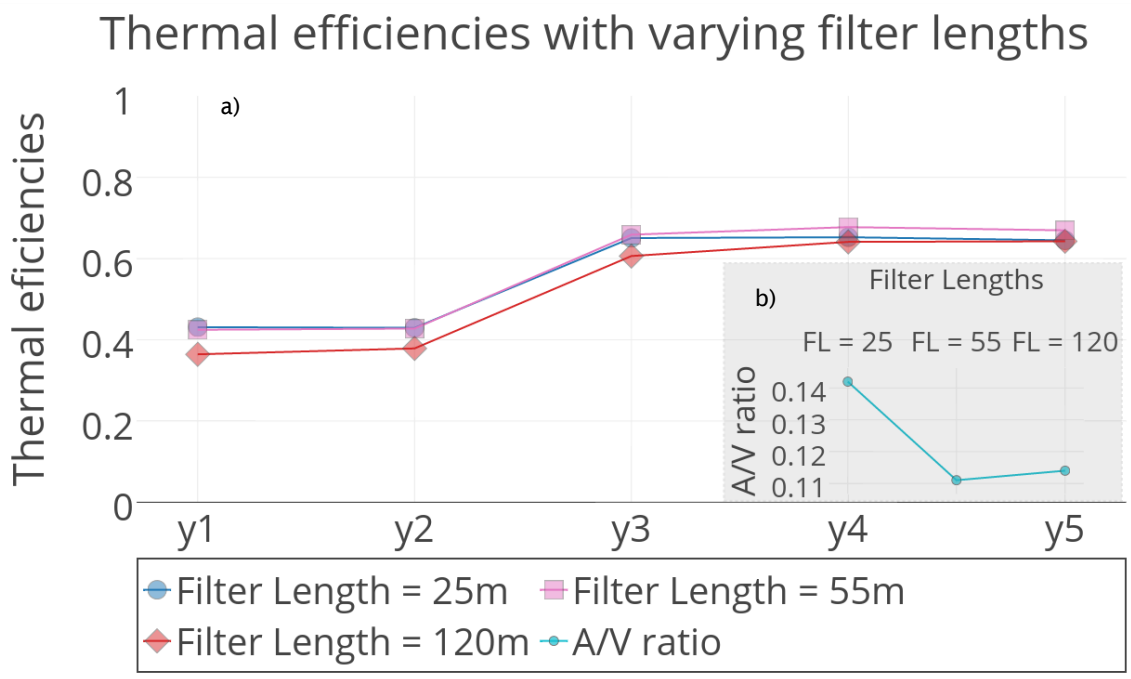

Figure 17: a) Thermal efficiencies with varying filter lengths over 5 recovery cycles. **b)** A/V ratio as a function of the considered filter lengths.

As observed from Figure 17a, the filter length of 55m yields the best thermal efficiencies for the later recovery cycles. This is due to the fact the most suitable filter length is based on the maximum storage volume, which is only reached in the later recovery cycles. This also explains that for earlier recovery cycles the results from the shorter filter length (25m) is showing comparable efficiencies with respect to the reference scenario. Similarly, for later recovery cycles the results from the longer filter length (120m) are closer to the results from the reference scenario than the results from the shorter filter length. Figure 17b supports the latter statement by showing that for the maximum storage volume the A/V ratio of the longer filter length is closer to that of the reference scenario than the A/V ratio of the shorter filter length.

4.1.4 Density driven flow

In Figure 18 the results of the thermal efficiencies with and without density driven flow can be observed. The first thing to note is that for each recovery cycle the efficiency is improved when the density and viscosity effects are not taken into account. The difference in efficiency compared to taking density driven flow into account is more pronounced with later recovery cycles. This is explained by the fact that for larger storage volumes at later recovery cycles, the warm front is more skewed.

4.1.5 Hydraulic conductivities

In Figure 18 the thermal efficiencies with three different conductivities are also shown. It is observed that increasing the hydraulic conductivities with a factor of 2.5 and 5 respectively reduces the thermal efficiency in the last recovery cycle by 18% and 48%. This is due to the fact that the warm water experiences less friction and can move more easily upward causing a more skewed front like in Figure 19. Note that the thermal efficiencies for the scenarios without density drive flow overlap. So the hydraulic conductivity only influences the losses caused by density and viscosity effects.

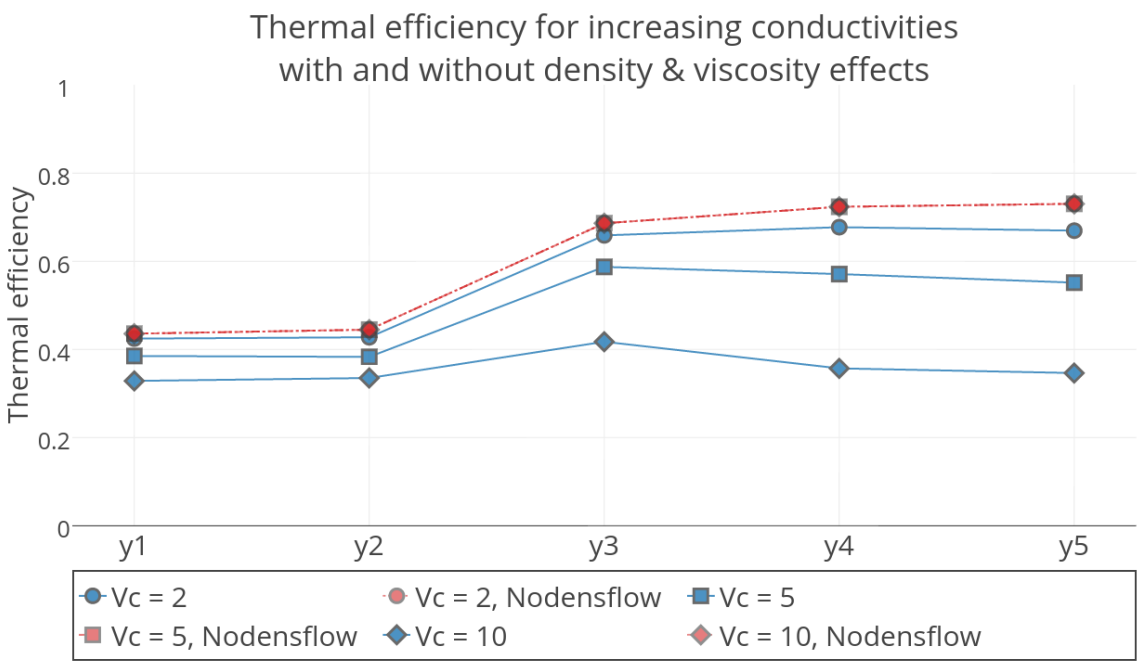

Figure 18: Thermal efficiencies with increasing vertical conductivities.

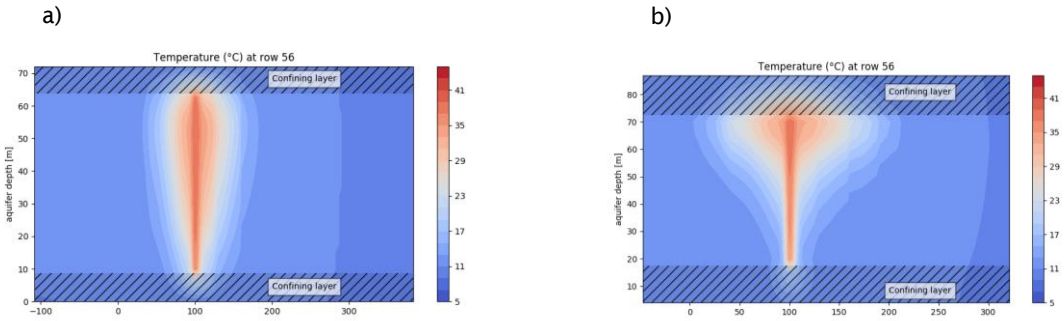

Figure 19: Cross section of the warm storage at the end of the last recovery cycle with **a)** Vc = 2m/day, and **b)** Vc = 10m/day

4.1.6 Comparing scenarios

The limiting factors for the ATES triplet system may be assessed from the performed sensitivity analyses. Remember that the scenarios are all considered to be in a temperate marine climate like in the Netherlands, so that the main difficulty lies within the storage of heat and not necessarily cold water. Now note the different thermal efficiencies for the scenarios described above, which are summarized in Figure 20 and consider the following:

- The first thing to note is that increasing the storage volume and hence improving the A/V ratio has the most influence in the first three recovery cycles.
- Secondly, increasing the injection temperature causes a larger temperature difference and a larger A/V ratio, which both reduce the thermal efficiency of the warm storage.
- Thirdly, the decreased filter length has a limited effect on the thermal efficiency. This is explained by the fact that the differences in A/V ratios are less pronounced compared to the differences in A/V ratio which are realized with doubling the GSA.
- The density flow is influencing the efficiency more strongly in the later cycles, but this effect is tempered by the relatively low vertical conductivities.
- Finally the conductivities strongly effect the thermal efficiency. The enhanced thermal losses caused by the higher hydraulic conductivities are caused by the density and viscosity effects.

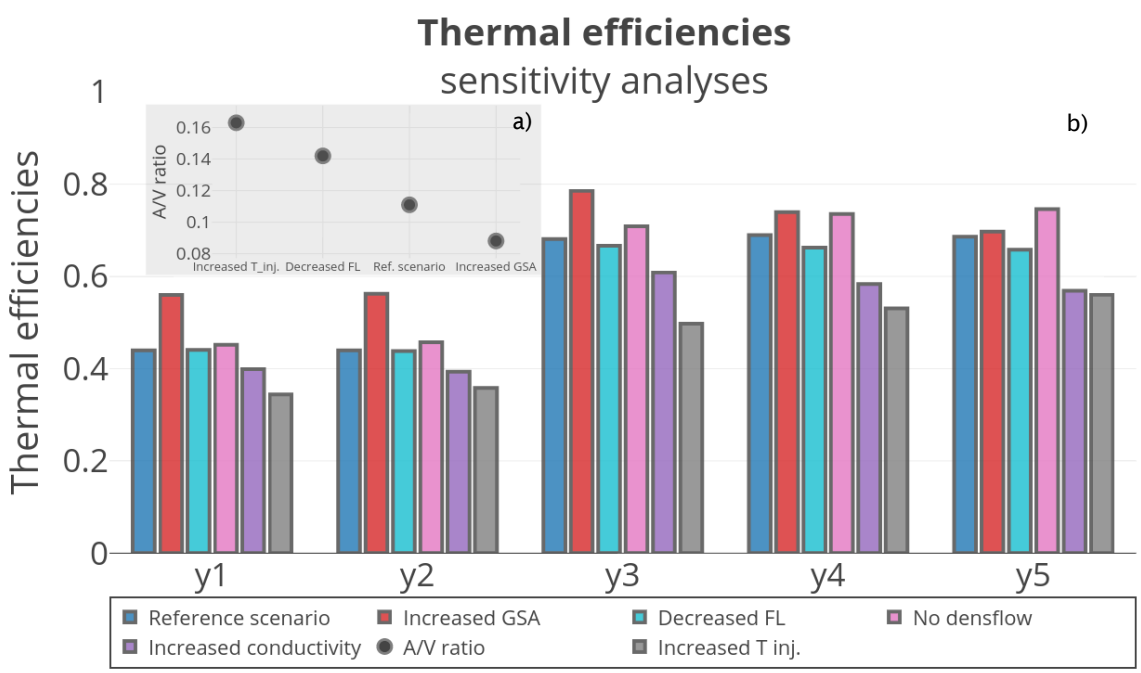

Figure 20: a A/V ratio with respect to the reference scenario, increased injection temperature, decreased filter length and increased GSA. **b)** Thermal efficiencies over 5 recovery cycles with respect to the following scenarios: reference scenario, increased GSA (80.000m^2), decreased Filter Length (25m), without density and viscosity effects, Increased Vertical conductivity (5m/day, with anisotropy of 5) and the increased injection temperature of the warm storage (50˚C).

4.1.7 Climatologic conditions

The climatologic conditions of each climate set and the minimum requirements regarding the solar heat collectors and the dry coolers are visualized in Figure 21. First some general remarks are made regarding the weather conditions and the ATES triplet performance. Subsequently the technical feasibility of an ATES triplet for each climate scenario is considered, supported by the outputs of CM1 in Figure 22.

4.1.7.1 General remarks

From Figure 21 the differences between the scenarios can be distinguished. The warmer climate (Sao Paulo), with relatively high yearly average air temperatures compared to the other scenarios will need an increased dry cooler capacity. Similarly the triplet system in a colder climate would require an increased area of solar heat panels, like in Umea. This has a number of reasons:

- First of all the demands for cooling in a warmer climate and similarly heating demands in a colder climate are enhanced.
- Apart from that, the warmer ambient groundwater in a scenario where more cooling is demanded will complicate the storage of cold water. This also holds for the storage of warm water in a cooler climate.
- Finally, the incoming solar radiation is less in colder climates, which makes it harder to gain heat from solar energy. As an illustration, consider Figure 21a where the incoming solar radiation per square meter over a year in Sao Paulo is almost twice as much as in Umea.

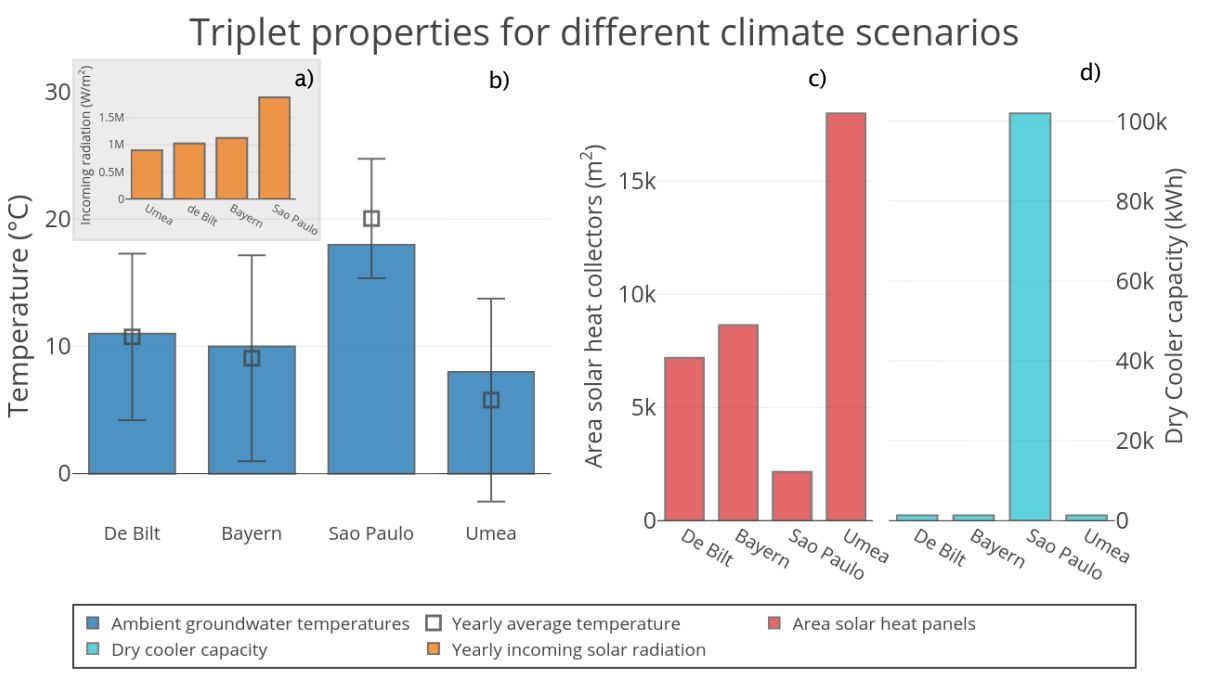

Figure 21: Triplet properties for different climate scenarios[1]: **a)** yearly incoming solar radiation per square meter, **b)** Average groundwater and air temperature ($\pm\sigma^2$) for the different climate scenarios, **c)** Area of solar heat collectors and **d)** cooling capacities.

4.1.7.2 Bayern

This set has similar yearly average temperatures and groundwater temperatures compared to the reference scenario. However, the variation around this temperature is larger, which causes higher demands for both cooling and heating. Hence the area of solar heat collectors is increased in order to provide in this demand. The increase in solar heat panels is however not very pronounced because of two reasons: the yearly incoming solar radiation is higher with respect to the reference scenario and the storage volumes are increased, limiting the thermal losses. Therefore the solar heat collector area and the dry cooler capacity needed to supply in heating and cooling demands will both fit on the roof of a building and the ATES triplet is technically feasible. Moreover, the building can have up to four stories before the technical limits of the ATES triplet are reached.

4.1.7.3 Sao Paulo

The outputs of this scenario support the statements in section 4.1.7.1 that the storage of cold water is much harder in a warmer climate. The most outstanding results are observed in Figure 22c, where the outputs of CM1 for Sao Paulo are depicted. Because there are only very few hours with temperatures low enough for charging the cold storage, the dry cooler must have 75 times the capacity of the dry cooler in the reference scenario in order to supply in a cooling demand for the upcoming warm season. As a result, the volume of the cold storage increases from approximately zero to 150.000m^3 in a few hours, resulting in pumping rates of 9.000m^3 per hour. Apart from that, the area of solar heat panels can be kept relatively low because of the high amount of incoming radiation, the lower demand for heating and the smaller difference between ambient groundwater and the warm storage temperature. So whereas the solar heat collector area and the dry coolers will fit on a roof, the pumping rates in and out the cold storage are demanding for 25 to 50 wells, considering typical pumping rates for ATES doublet systems. Therefore the spatial planning of the wells is technically unfeasible and an ATES triplet can't be realized in a climate as in São Paulo.

[1] *N.b. the minimum temperature at which the cold storage is charged (see section 2.1.1.1) is adjusted to 9° for the triplet system in Sao Paulo, because there are no hours at which the air temperature drops below the 4 °C. The injection temperature is subsequently set to 10°C.*

4.1.7.4 Umea

Contrary to the São Paulo climate scenario, this dataset yields relatively cold ambient air and groundwater temperatures. Now the challenge is storing warm water instead of cold. This can be seen from Figure 21, where the area of solar heat panels is required to be approximately 2.5 times the area in the reference scenario. This increase in the area of solar heat panels is necessary in order to prevent the warm well temperature from dropping below the cut-off temperature. However, the area of solar heat collectors is still lower than the GSA and the ATES triplet can be realized for buildings up to two stories high.

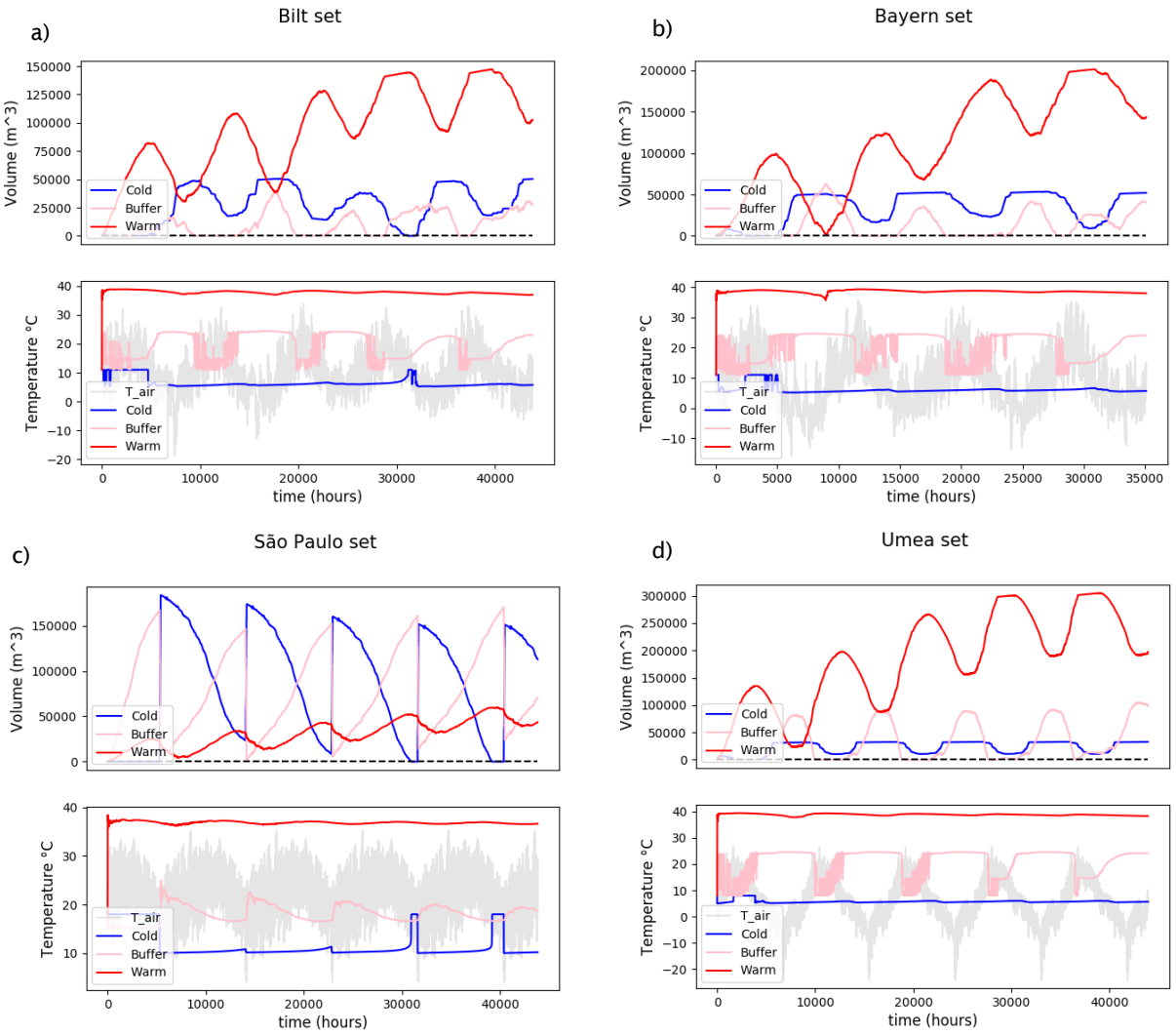

Figure 22: Volume and temperature outputs of CM1 for **a)** De Bilt climate, **b)** Bayern, **c)** São Paulo and **d)** Umea climate conditions.

4.2 Test case

In order to answer the main research question, which regards the feasibility of a thermally self-supporting ATES system, the test case is considered. First the technical feasibility is tested, then the environmental aspects are treated and finally the economic feasibility is considered.

4.2.1 Technical feasibility

The minimum solar heat collector area and dry cooler capacity required to meet the conditions for the technical feasibility are determined empirically, by running the model with different property sets. The settings which are schematically depicted in Table 3, show that the solar heat collector area is much less than the GSA. Moreover, the ATES triplet could provide in the heating and cooling demand of a building up to 4 stories high. The implementation of these settings to CM3 leads to the outputs visualized in Figure 23. As can be observed from Figure 23c, the temperature of the warm storage does not drop below the cut-off temperature so the second condition for the technical feasibility has been met as well.

Because the yearly average cooling demand is much lower than the heating demand, the corresponding storage volume for the cold storage is much lower than for the warm storage. As a consequence it can be observed from Figure 23b that the storage is empty at the start and in the 4th recovery cycle. Nonetheless the storage is able to provide effective cooling with ambient groundwater temperatures. This supports the simplification for the technical feasibility that the main challenge is storing warm instead of cold water.

Finally consider the buffer storage, which temperature varies between the 15˚C and 25˚C. An important thing here is to register whether the buffer storage is not expanding too much. Whereas the warm and cold storage are limited by a maximum thermal energy capacity, which can be observed by the thresholds in Figure 23a-b, the thermal energy of the buffer storage is not restricted. However, the volume of the buffer storage has expanded from 0 to 50.000m^3 in 5 years, which is relatively low compared to the expanding of the warm storage (0 to 120.000m^3 in 5 years). Neither do the cold and warm storage seem to interfere with each other in a negative way. This is supported by Figure 24 where the temperature cross section is presented at the time when the thermal energy and volume of the warm storage are at maximum.

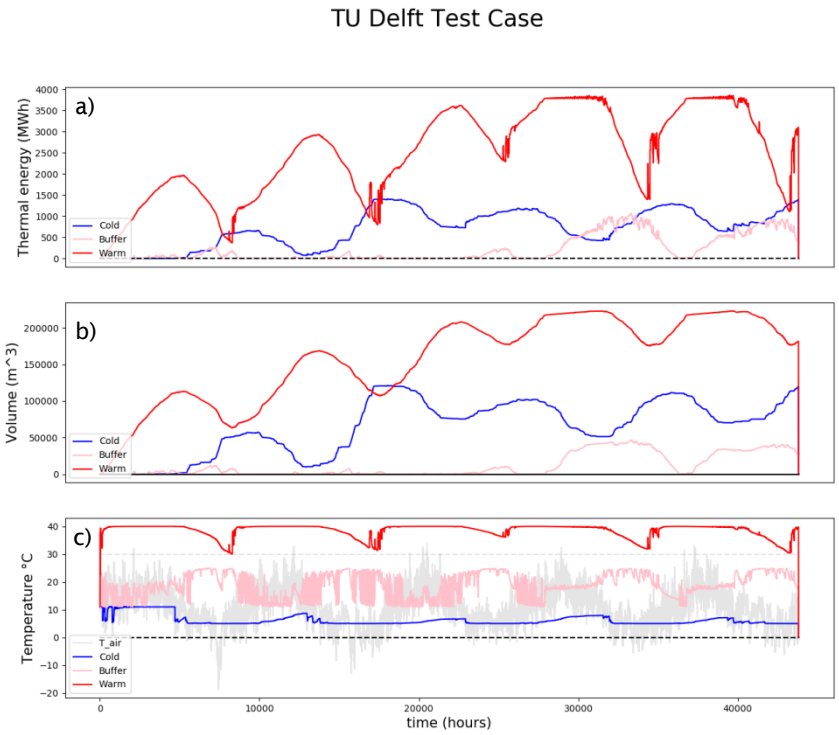

Figure 23 : Results of test case TU-Delft campus. **a)** Thermal energies (MWh), **b)** Volumes (m^3), **c)** Extraction temperatures (˚C) where the cut-off temperature is represented by the gray dashed line.

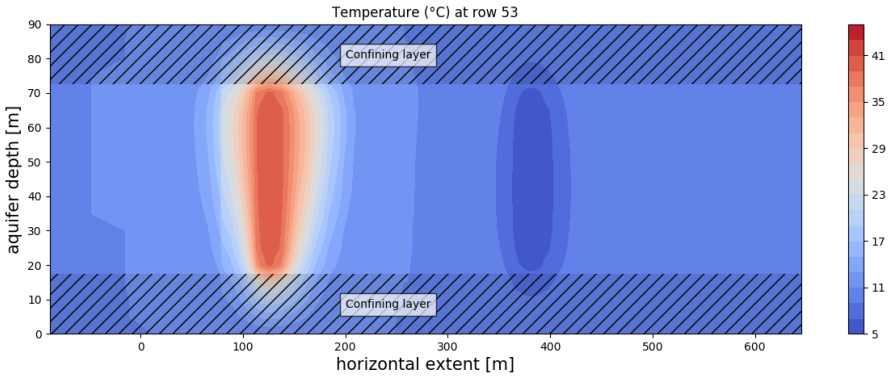

Figure 24: Cross section of the aquifer with temperature profiles at the time when the thermal energy of the warm storage is at maximum.

4.2.2 Environmental analysis

The results of the environmental analysis for the test case are presented in Figure 25, where the benefits of an ATES triplet are visible. Whereas the pumping rates are significantly higher considering the triplet system, the reduction in energy use is the most convincing. The triplet respectively uses 2% and 9% of the energy a conventional system and a doublet would use. This can be explained by the fact that the energy used in a triplet system is merely used for the pumping of water, whereas the other systems need energy for active heating and cooling.

Considering the CO_2 emissions the differences are a bit less pronounced. This is due to the fact that 1MWh of energy produced by using gas will lead to less CO_2 emissions compared to the situation where electricity was used to produce this energy. Nonetheless the results confirm that the CO_2 emissions are decreased to respectively 3.5% and 8.5% of the emissions from a conventional system and an ATES doublet. This supports the hypothesis on the prospects of an ATES triplet in Figure 3.

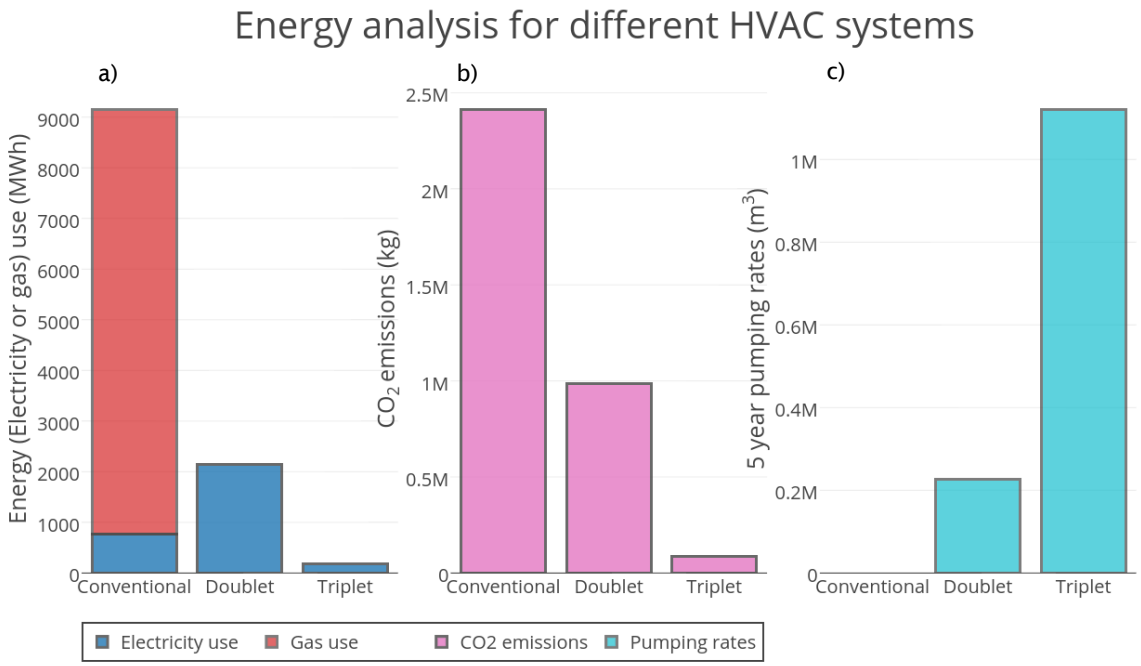

Figure 25: Analysis of **a)** energy use, **b)** CO_2 emissions and **c)** pumping rates of an ATES triplet over 5 years compared to a conventional and an ATES doublet system.

4.2.3 Economic feasibility

Now that the benefits considering energy use and CO_2 emissions of the triplet system are clear, the total costs of ownership (TCO) and operational costs are considered in order to determine the economic feasibility. In Figure 26a the TCO over 30 years with respect to different equity capital (EC) are presented and Figure 26b shows the operational costs over 5 years.

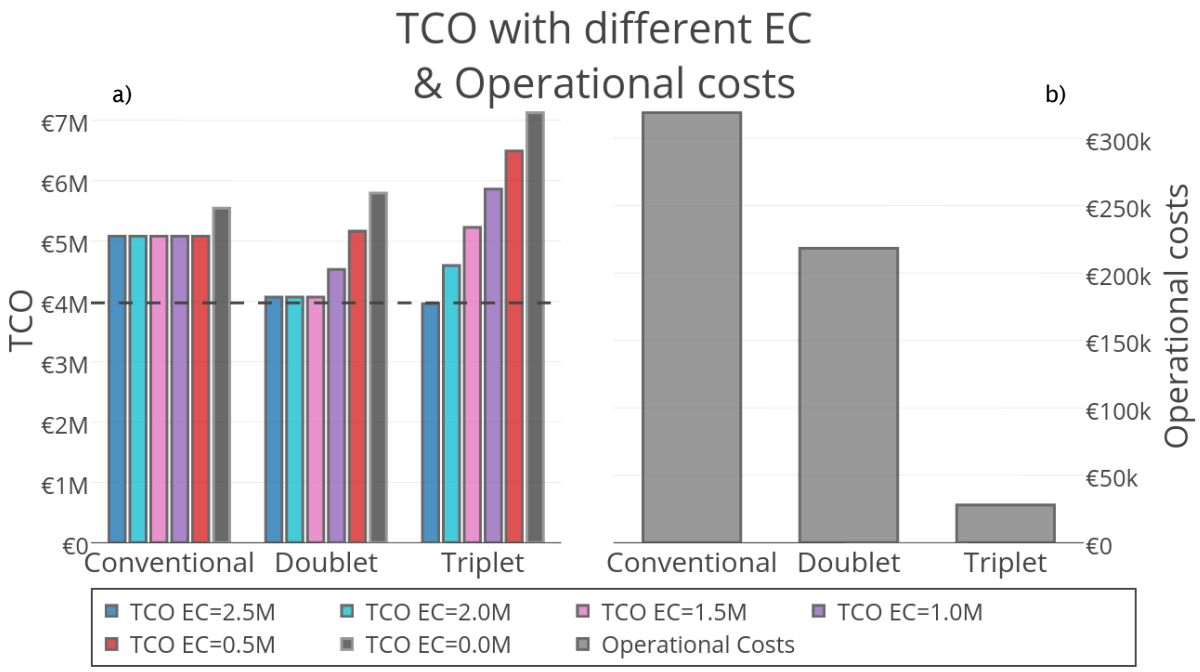

Figure 26: a) TCO of the different space conditioning systems over 30 years. Dashed line shows that for EC=€2.5M, the triplet system has a lower TCO. **b)** Operational costs of a conventional system, an ATES doublet and an ATS triplet over 5 years.

From Figure 26b it is observed that the gains in operational costs are very convincing, similar to the additional cuts in energy use and CO_2 emissions. Whereas an ATES doublet would use 68.4% of the operational costs a conventional system would use, the ATES triplet uses only 8.8% of the operational costs. However, due to the high installation costs for the solar heat panels and the extra wells, the cuts in TCO are less pronounced or not present at all (Figure 26a). When there is no equity capital, the conventional system appears to still be the cheapest option. However, when there is an equity capital of €2.5million euros, the triplet system will indeed show a reduced TCO with respect to the conventional and the doublet system. In addition, the cost-recovery times are identified to be respectively 23 years and 29 years with respect to the conventional and the ATES doublet system. Therefore the realization of the ATES triplet in the test case is economically feasible when there is an EC of €2.5million.

5 Discussion

Discussion of the used models, calculation methods, the sensitivity analyses and the test case.

5.1 Anomalies in the calculation methods

5.1.1 Temperature representation

The main weakness of the triplet model is the representation of the storage temperatures and the thermal losses. In Figure 27 the temperature profiles of the warm storage of the triplet model and the subsurface model are sketched. Whereas the subsurface model distinguishes varying temperature profiles, the triplet model regards an average storage temperature. This will lead to anomalies in the communication between the triplet and subsurface model.

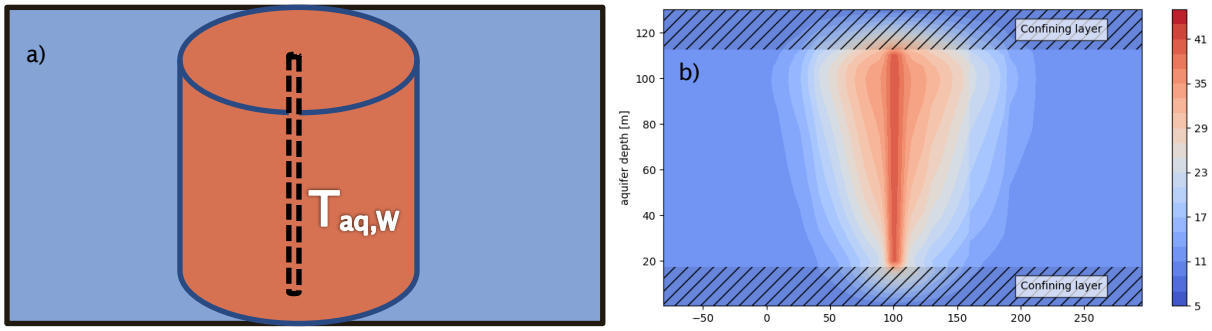

Figure 27: Temperature representation of **a)** triplet model, **b)** subsurface model.

5.1.2 Pumping rates

The temperature at the well dictates how much volume is needed to provide in a heating or cooling demand. As can be seen from Figure 27b, the temperature at the well is different from the temperature at the edges of the warm storage. The temperature at the well also deviates from the average warm storage temperature which is presented by the triplet model (like in Figure 27a). Therefore the temperature at the well is not representing the right temperature, which leads to anomalies in the pumping rates which are calculated by the triplet model. These pumping rates are exported to the subsurface model in CM2, which therefore shows anomalies in the storage temperatures as well. The anomalies are mainly present in CM1 and CM2, but are fixed by using CM3.

5.1.3 Thermal energy

The thermal energy depends on the temperature level of the storage as in equation (10). This approach is valid as long as the temperature level $T_{aq,w}$ represents the average temperature of the injected volume as in CM1 and CM2. When the triplet and subsurface model are coupled in CM3, $T_{aq,w}$ represents the temperature at the well. The thermal energy is then regarded as the thermal energy of warm storage where all of the warm storage would have the same temperature as the temperature at the well. Because the temperature at the well is higher than at the edges due to the thermal losses (see Figure 27b), this causes an overestimation of the thermal energy in the warm storage.

5.1.3.1 Useable & useless thermal energy

From the outputs of CM3, the distinction between useable and useless thermal energy can be made. For the warm storage useable energy is defined as the energy of the volume with a temperature higher than, or equal to the cut-off temperature. For the cold storage a similar distinction is made by implying that the most efficient cooling is realized with water colder than 6˚C. Consequently the energy of the volumes yielding water below 6˚C is defined as useable thermal energy for the cold storage. The difference between the thermal energy calculated from equation (10) in the triplet model and the useable thermal energy is defined as the useless thermal energy. The overestimation of the thermal energy in the triplet model is visualized in Figure 28a, where the difference between useable (black line) and useless thermal energy (red shaded area) is shown for the warm storage. The storage of heat is limited by the maximum thermal energy implied in the

triplet model. As a consequence the useable thermal energy at later recovery cycles doesn't cover the yearly average heating demand. This gives rise to the thought whether the thermal energy should be limited by the useable energy inside the wells instead of the thermal energy as described by the analytical model.

In Figure 28b the results of this revised conditions on the thermal energy of the warm storage are shown. At first glance, these results seem to improve the results on thermal energy since the useable energy now reaches its maximum each recovery cycle after the first. However, Figure 28c shows the results of the pumped volumes between the storages, where it is observed that the warm and cold storages are steadily expanding. This makes sense by arguing that there will always be less energy pumped out of the storage than into it due to thermal losses during storage. Therefore, the aquifer will steadily warm up over time, which may lead to a reduced efficiency of the cold storage. On the other hand, the cold storage is also expanding, so to what extent this will give rise to problems concerning the feasibility of an ATES triplet is hard to make up from Figure 28c.

5.1.4 Expanding of warm storage

Additional runs over more than 5 years are applied in order to visualize the effects of constantly pumping more heat and cold water in than out of the aquifer. The effects are visualized by plotting the maximum horizontal distance of the 12°C contour line – henceforth denoted as the thermal front - with respect to the warm well. In Figure 29 the distance of the thermal front with respect to the warm well is strongly increasing in the first years. At later time the difference gets smaller by the effects of dispersion and conduction on the increasing surface of the thermal front, which causes the thermal front to move more slowly away from the warm well. Because the thermal front doesn't expand significantly anymore from later years on, it is stated that restricting the subsurface model to the useable energy instead of the analytic outputs will yield better performances of the triplet system.

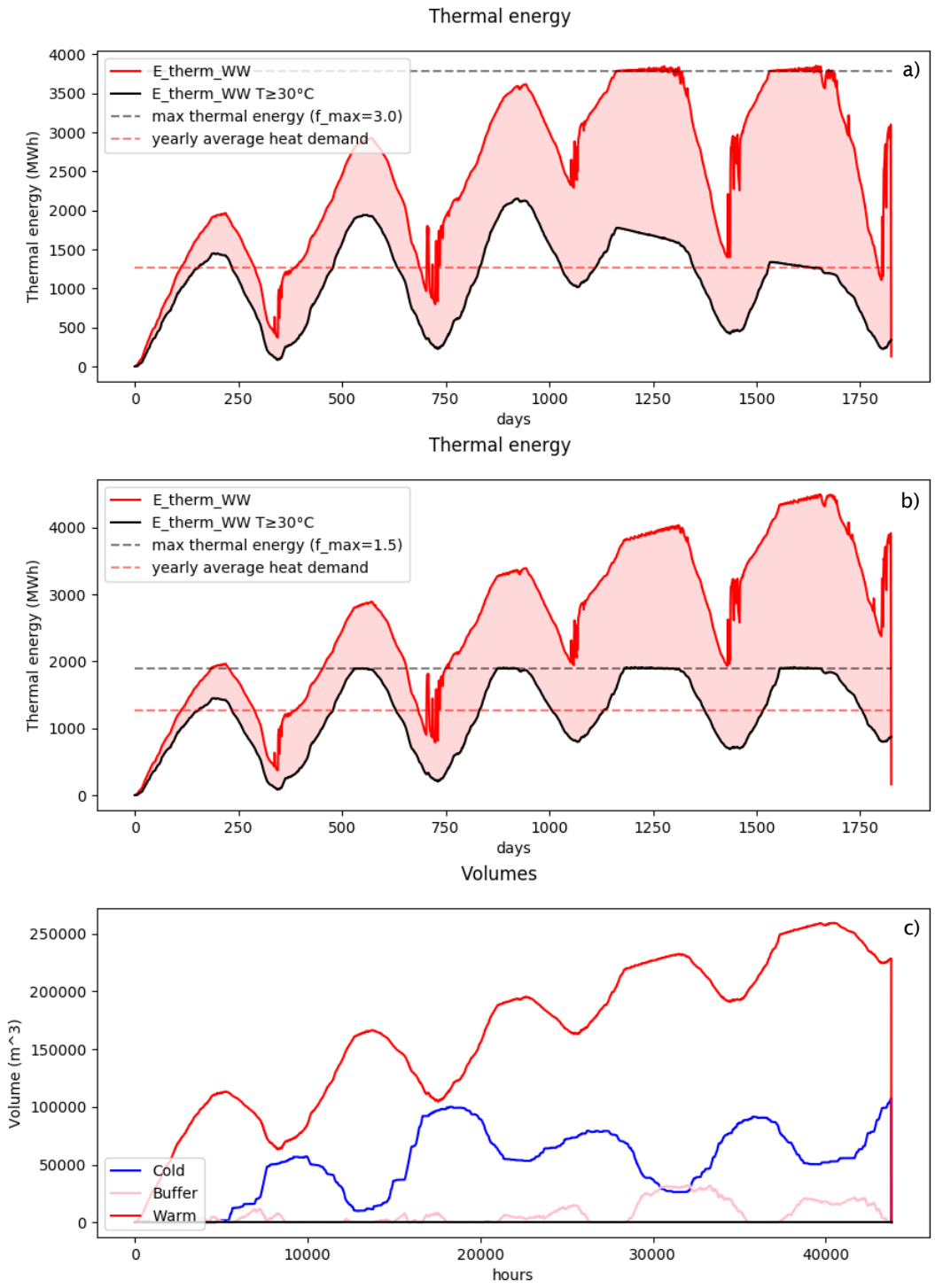

Figure 28: Useable and useless energy modeled with condition for maximum thermal energy implied on **a)** triplet model outputs **b)** subsurface model outputs and useable thermal energy. **c)** Volumes of the warm buffer and cold storage. The red shaded area is the useless thermal energy.

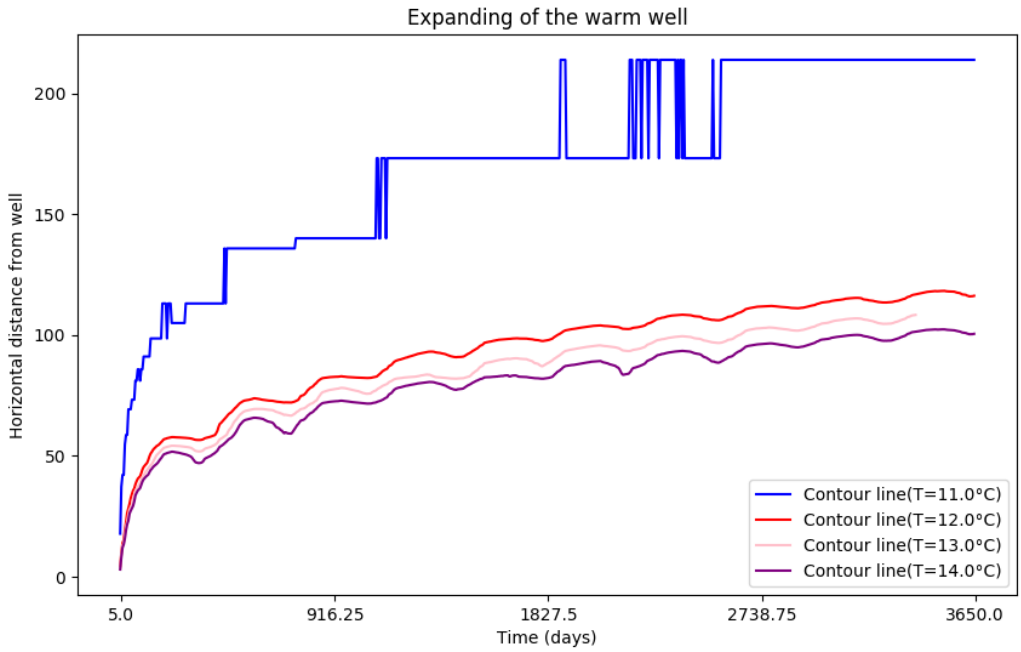

Figure 29: Distance of the 11˚C, 12˚C, 13˚C and 14˚C contour lines with respect to the warm well.

5.2 Sensitivity analyses

5.2.1 Reference scenario

The 3mE building on the TU-Delft in the Netherlands, which is used as a reference scenario, is built in 1953 (Delft 2013) which allows for stating that the isolation techniques are outdated compared to current techniques. Therefore the used heating and cooling demands per square meter are higher than they would be for buildings which are newly built. As an illustration the yearly average heating demand for current new built buildings is reduced to almost a third of the yearly average heating demand used for the reference scenario(Meijer et al. 2009). Since the main difficulties of the ATES triplet regard the storage of warm water, the potential of an ATES is almost three times as high for new buildings. Therefore an ATES triplet can be realized for new, well isolated buildings up to 12 stories high, based on the outputs of the reference scenario.

5.2.2 Building sizes

The used building sizes are relatively large compared to domestic buildings or typical offices in the Netherlands. Applications of the considered GSA's can be found in large buildings, or groups of buildings. For smaller storages than the storage in the reference scenario the thermal losses of the warm storage will further be enhanced, reducing the potential of an ATES triplet.

5.2.3 Injection temperatures

The results of the injection temperatures are presented in terms of the temperature as a function of the volume fraction for each recovery cycle (Figure 16) instead of the thermal efficiencies. This is done in order to show the decline in warm storage temperature over time with different injection temperatures. Apart from that, the results are calculated using CM2 and the anomalies in the pumping rates occur, as described in section 5.1.2. The anomalies are enhanced because the cut-off temperature is more quickly reached for lower injection temperatures so that the triplet model resets the storage temperature and volume of the warm storage.

5.2.4 Filter Lengths

Whereas the filter lengths are now chosen in order to visualize the effect of the geometry of the storage on the efficiency, the filter lengths usually depend on the availability of geological suitable aquifers in the subsurface. For example: The confined aquifers under the TU-Delft are either 20, 50 or 150m thick (Hacking 2017). So if the storage needs to be confined, the filter length consequently is a property of the considered aquifer and cannot be assigned.

5.2.5 Density driven flow & Hydraulic conductivities

It is shown that the effect of temperature dependent viscosity and density is limited for low conductivities, but has a higher impact on the thermal efficiency for higher conductivities. Therefore the aquifers with low hydraulic conductivities (fine-sanded aquifers) show the highest potential for an ATES triplet. The conductivities used in the reference scenario are relatively low compared to typical Dutch coarse-sanded aquifers which are currently widely used in ATES doublet realizations.

5.2.6 Climatologic conditions

5.2.6.1 Potential in perspective of previous work

Considering the climatologic conditions, the results mostly follow previous work on the potential of ATES doublets worldwide (Bloemendal et al. 2015). The results of this work are visualized in Figure 13, where the locations of the used climate sets are added. Now consider the area of solar heat panels and capacity of the dry coolers (see Figure 21) as a measure for the potential of an ATES triplet system. The following potential is assessed for the different climate sets compared to the previous work by (Bloemendal et al. 2015):

- The weather conditions in de Bilt clearly yield the best potential, as the area of solar heat panels and dry cooler capacity which are necessary are the lowest. This corresponds to the potential sketched by (Bloemendal et al. 2015).
- For the triplet system in Bayern, the area of solar heat panels must slightly be increased in order to meet the technical feasibility conditions, which reduces the potential of the triplet for a small part. This also follows the potential sketched in Figure 13.
- As for the Sao Paulo dataset, the potential of a triplet is worse than expected from Figure 13. The low potential is mainly due to the required dry cooler capacity and the need for multiple wells. The discrepancy with Figure 13 is probably due to the fact that (Bloemendal et al. 2015) looked at the potential of ATES doublet systems, where in contrary to the ATES triplet, cooling can be provided by making use of the heat pump.
- Finally, the Umea dataset yields a moderate potential as the area of solar heat panels needs to be increased, whereas the dry cooler capacity may be decreased. Therefore it seems to have a better potential then what was expected from Figure 13. This is probably due to the fact that the geo-hydrological conditions, which are not incorporated in detail by making use of CM1, are of low potential here.

5.2.6.2 Future climate

In section 4.2.1 it is shown that the main challenge regarding the ATES triplet in the Netherlands is storing hot water instead of cold. Note however that the climate is changing and that the average yearly air temperature is expected to increase (IPCC 2011). This will firstly cause the demand for heating to be lower, secondly there is more time to charge the warm storage (more efficiently due to the reduced difference between the collector plate temperature and the air temperature) and thirdly the ambient groundwater temperatures will warm up which reduces the thermal losses. Hence the potential for an ATES triplet in the Netherlands is expected to increase in the coming years, since the problems regarding the storage of warm water will decrease. Note however, that the potential decreases when the temperature raises too much and the problems will shift to the storing of cold water instead of warm, like in São Paulo.

5.3 Test case

5.3.1 Technical feasibility

One of the requirements to achieve technical feasibility considers the solar heat collectors. As the different settings regarding solar heat collector area were tested, the maximum area of solar heat panels - which is equal to the roof area – was not enough to prevent the temperature at the warm well from dropping below the cut-off temperature. So either the yearly average demand for heating should be lowered by another 20%, or the area of solar heat panels should be increased by placing the collectors elsewhere. Therefore the results presented in section 0 are leading to a feasible triplet scenario, provided that the demand for heating is lowered by another 20%. This can be achieved by improving the insulation of the building.

5.3.2 Environmental analysis

The parameters used in the environmental and economic performance show the average value of a possible range of parameter values. Therefore the presented values for CO_2 emissions and energy use can deviate for other applications of the ATES triplet, doublet or conventional systems. Apart from that, note that only the CO_2 emissions and energy use for the operational conditions are taken into account. So the CO_2 emissions and energy use over the lifecycle of all the properties of the ATES triplet, doublet and conventional system are not taken into account.

The operational costs, energy use and CO_2 emissions are only investigated for the test case. When the conditions for the realization of an ATES triplet are different, like sketched in the Sensitivity analyses, the number of solar heat collectors and the capacity of the dry cooler have to be adjusted in order to meet the conditions for the technical feasibility. This will cause the pumping rates to be different and consequently influences the environmental performance. However, since the ATES triplet only requires energy to pump water from one storage to another the environmental performance will exceed the environmental performance of the ATES doublet and conventional system for all conditions which are technically feasible. The bigger challenge lies in the economic feasibility of an ATES triplet.

5.3.3 Economic feasibility

Because the interest rates on debt capital are much higher than on equity capital, the economic feasibility depends on the equity capacity to finance a new space conditioning system. In this case it is shown that an equity capital of €2.500.000,- is required for economic feasibility. However, the subsidies on improved cuts in CO_2 emissions and energy use are not taken into account here. To support the thoughts on subsidies for energy reducing systems like the ATES triplet, note that the Dutch government is planning to cut out all the gas use by 2050 (Rijksoverheid 2016). Apart from that, the main costs for the triplet system are incorporated in the installation of the solar heat collectors. With improving techniques it is expected that these costs will decrease in the coming decades, improving the economic potential of the triplet system.

5.3.4 Spatial planning of storages

To what extent the storages are actually influencing each other at what distance and which spatial planning limits the interaction between the storages the most, is also left out of consideration. Previous work by (Sommer et al. 2015) has shown what the ideal pattern is for ATES doublets, but a triplet system yields deviating injection temperatures. Intuitively one my conclude that the warm and cold well must be separated as far as feasible, but to what extent the warm well may benefit from the buffer well is not quantified. In order to do so, additional research is necessary with respect to spatial planning and interaction of wells for a triplet system.

6 Conclusion

Conclusions and answers to the research questions

The main aim of this research is to investigate the feasibility and potential of a thermally self-supporting ATES; an ATES triplet. The feasibility is tested by making use of a test case, situated on the TU-Delft (the Netherlands) campus above a fine-sanded aquifer in a marine climate. It is shown that for a large building (GSA 40.000m^2 or bigger), the ATES triplet is technically and economically feasible provided that there is an equity capital of €2.5M. Hence the ATES triplet can be realized for well isolated buildings up to four stories high. The CO_2 emissions and operational costs are both reduced to less than a tenth of the values from the ATES doublet and conventional system. In addition, the costs over the time of ownership are reduced as well.

6.1 Storage volume and building size

Building sizes are directly related to the amount of heating and cooling which is demanded and are hence related to the storage volumes. The bigger the storage volume is, the lower the A/V ratio of the storage. This causes the thermal losses to decrease with increasing building sizes. So with increasing building sizes less solar heat collectors are required per m^2 of building area and the potential of the ATES triplet increases.

6.2 Aquifer properties

The effect of two aquifer properties on the ATES triplet potential are investigated:

- The filter lengths of the storages
- The hydraulic conductivities

The filter length of the storages depends on the available confined aquifer thickness. An ideal filter length is identified for each cylindrical shaped storage volume. The ideal filter lengths minimizes the A/V ratio and hence the thermal losses. The more the filter length deviates from the ideal filter length, the lower the potential of the ATES triplet is.

The aquifer composition determines the hydraulic conductivities in the subsurface. Hydraulic conductivities corresponding to fine-sanded aquifers show the highest potential for the realization of an ATES triplet. With lower conductivities, the water will experience more friction and the effect of density driven flow and temperature dependent viscosity are limited. Aquifers with higher conductivities corresponding to coarse-sanded aquifers, show reduced thermal efficiency and hence a lower potential for the realization of an ATES triplet.

6.3 Climatologic conditions

Four different climate sets have been analyzed in order to assess the potential for an ATES triplet in different climates. The highest potential is found in temperate marine climates like in the Netherlands, where an ATES triplet can be realized for buildings up to five stories high. The lowest potential is found in subtropical climates, where it is hardly feasible to acquire and store cold water to provide in the high cooling demand. In colder climates the potential is reduced, but technically feasible for buildings up to two stories high. Finally, in continental climates the ATES triplet can be realized for buildings up to four stories high, which is lower than the potential in a marine climate.

6.4 Economic and environmental benefits

The ATES triplet only requires energy for pumping water between the storages and the building, whereas the ATES doublet and conventional systems need energy to produce heat. Therefore the energy use of a building is reduced to 8.5% of the energy an ATES doublet would use. Consequently the CO_2 emissions of an ATES triplet are reduced to respectively 3.5% and 8.5% of the emissions a conventional system or an ATES doublet would emit. So the ATES triplet shows great improvements on energy use and CO_2 emissions, which supports the aims of developing an ATES triplet.

Similarly to the CO_2 emissions, the operational costs of an ATES triplet are reduced to respectively 5.9% and 8.5% of the operational costs a conventional system or an ATES doublet would use. However, the installation costs of an ATES triplet are higher than the installation costs of an ATES doublet and of a conventional system, due to expensive solar heat collectors. The TCO are lower when there is enough equity capital to cover a part of the installation costs. Therefore the economic benefits of an ATES triplet are most pronounced when there is sufficient equity capital.

7 Appendix

7.1 Appendix A

Financiële Kentallen							
\		doublet		"Triplet" of "Doublet"		Delta P doublet	0.0408
Boorlengte		**150**	**m**			Delta p triplet	0.0612
Boorputdiameter		**1.00**	**m**				
Debiet (Q)		**200**	**m3/h**				
Aantal doublet(ten)		2					
Lengte terreinleidingen		**100**	**m**				
Vermogen bron (P)		**8.16**	**kW**				
totale kosten		**€ 861,980.01**					
Diameter range		**Euro/m boorgat**	**put behuizing**				
0.4	0.6	€400	€3,000				
0.6	0.8	€550	€5,250				
0.8	1.0	€750	€7,500				
1.0	1.2	€900	€11,250				
1.2	>	€1,250	€15,000				
Rekenwaarden		**€750**	**€7,500**				
Terreinleidingen		**Euro/m terreinleiding**					
		€100					
TSA		€4,285					
Debiet range		**Euro/pomp**	**frequentie omv.**	injectie kleppen			
0.0	50.0	€7,500	€4,000	€4,000			
50.0	100.0	€10,000	€5,000	€5,000			
100.0	150.0	€15,000	€6,000	€6,000			
150.0	200.0	€25,000	€7,000	€7,000			
200.0	250.0	€35,000	€8,000	€8,000			
250.0	300.0	€50,000	€9,000	€9,000			
Rekenwaarden		**€7,500**	**€7,000**	**€7,000**			
* Per doublet is een TSA nodig en zijn twee bronpompen + frequentie omv. benodigd							
Kosten							
Kosten boring incl behuizing per double		€240,000	Euro				
Kosten leidingwerk		€10,000	Euro				
Kosten pompen, tsa en freq. omv. per c		€86,000	Euro				
Kosten per doublet		**€326,000**	Euro				
Proefboring ja/nee		ja		"ja" of "nee"			
Kosten proefboring		€60,000	Euro		1/4 bronkosten		
Kosten technische ruimte		€57,333	Euro				
Totale kosten							
Aanleg		**€783,618**	Euro				
Vergunning, voorontwerp, effectenstudie		€39,181	Euro		Variërend percentage van aanle		
DO, bestek		€39,181	Euro				
Kosten onderhoud		€11,754	Euro/per jaar		Variërend percentage van aanlegkosten met een minimum van 7500		
Extra kosten aanpassingen zout water							
Pompen		€21,500	Euro		25%		
Technische ruimte		€5,733	Euro		10%		

Figure 30: Assumptions concerning the costs of the development of a well

Column1	Column	Column
P_dc	1360 kW	
P_pt	5000 kW	
Max warmtevraag	1780 kW	
Max koelvraag	1720 kW	

Regeneratie	Ruimtebeslag		Rendement			Economisch								
	Technische ri	Dak	energieinvoe	rend-warm	rend-koud	rend-wtw	kosten	kosten : A	kosten : B	Minimumprijs	subsidie	A*P^B	Minimum	
Droge koeler	0	0.1	elektriciteit	20	20	nvt	A*P^B	682.9	-0.309	80	0.1122	€ 6,347.76	€ 108,800.00	
Droge koeler tbv compressiekoeling	0	0.1	elektriciteit	15	15	nvt	A*P^B	341.45	-0.309	40	0	€ 3,412.76	€ 54,400.00	
Natte koeler	0	0.03	elektriciteit	25	25	nvt	A*P^B	1000	-0.309	120		€ 9,994.90	€ 163,200.00	
LBK	0	0	elektriciteit	0	15	nvt	A*P^B	50	0	50				
Zonnecollector	0	25	elektriciteit	100	1	0.58	A*P^B	1888.1	-0.469	400		€ 102,527.87	€ 2,000,000.00	
Asfaltcollector	0	25	elektriciteit	100	3	nvt	A*P^B	211.74	-0.069	115				
Energydak	0	25	elektriciteit	100	3	nvt	A*P^B	323.06	-0.107	150				
Oppervlaktewater	0	0	elektriciteit	100	100	nvt	A*P^B	300	0	300				
TSA warmte invang			nvt				A*P^B	1308	-0.428					
Geen, regeneratie	nvt	nvt		nvt	nvt	nvt	nvt	0	0	0				
	Technische ri	Dak	energieinvoe	rend-warm	rend-koud	rend-wtw	kosten	kosten : A	kosten : B	Minimumprijs	subsidie			
Warmtepomp	0.04	0	elektriciteit	0	0	3	A*P^B	2137.4	-0.408	200	0.1122			
Bio WKK	0.025	0	(Bio)brandst	0	0	0.5	A*P^B	8607	-0.278	840	0			
Gas WKK	0.025	0	gas	0	0	0.5	A*P^B	7639	-0.34	625	0			
Geen-basis	nvt	nvt	geen	0	nvt	nvt	nvt	0	0	0	nvt			
Energieopwekker aanvullend-warm	Ruimtebeslag		Rendement			Economisch								
	Technische ri	Dak	energieinvoe	rend-warm	rend-koud	rend-wtw	kosten	kosten : A	kosten : B	Minimumprijs	subsidie			
CV ketel-gas	0.03	0	gas	0.9	nvt	0.85	A*P^B	258.22	-0.195	60	0	€ 1,111.28	€ 106,800.00	
CV ketel-E	0.025	0	elektriciteit	0.9	nvt	0.85	A*P^B	308.03	-0.271	70	0			
(Bio) Olie-ketel	0.025	0	Palm olie	0.85	nvt	0.85	A*P^B	3772	-0.601	70	0			
Olie-ketel	0.025	0	Olie	0.85	nvt	0.85	A*P^B	3772	-0.601	70	0			
Restwarmte/SV	0.025	0	warmte	1	nvt	1		100	0	100	0			
Restwarmte/SV pieklast	0.025	0	warmte	1	nvt	1		150	0	150	0			
Geen, monovalent systeem	nvt	nvt	geen	nvt	nvt	nvt	nvt	nvt	nvt	nvt	nvt			
Energieopwekker aanvullend-koud	Ruimtebeslag		Rendement			Economisch								

Figure 31: Assumptions concerning the investment costs of the different aspects of conventional, doublet and triplet space heating.

TKI OMALA - LA			
Versie	1.1		
Opsteller	Martin Bloemendal		19-12-2016
Borging			
Aanpassing na borging/def			
Algemeen			
Levensduur installatie		30	jaar
Afschrijftermijn 1 (civiel)		20	jaar
Afschrijftermijn 2 (WTB)		10	jaar
Afschrijftermijn 3 (elektra)		7.5	jaar
Afschrijftermijn 4 (kort)		1	jaar
Startjaar (Jaar 0)		2015	
Eindjaar		2045	
Prijsindexen			
Prijsindex algemeen		2.00%	
Prijsindex elektriciteit		6.00%	
Prijsindex gas		6.00%	
Water- en Energieprijs			
Gas		€ 0.45	/Nm^3
Elektriciteit		€ 0.10	/kWh
Water		€ 1.75	/m^3
Financiering			
Inbreng eigen vermogen		€ 2,500,000	
Rente op eigen vermogen		2.00%	
Rente op vreemd vermogen		6.50%	
Tarieven Menskracht			
Ontwerp		€ 120	/uur
Voorbereiding financiering		€ 80	/uur
Vergunningen		€ 100	/uur
Aanleg/bouw		€ 80	/uur
Oplevering		€ 80	/uur
Bedrijfsvoering en Onderhoud		€ 80	/uur
Beheer		€ 80	/uur

Figure 32: Assumptions concerning economic aspects

Totaal					€ 283,500.00
Investeringskosten					
Omschrijving	**Aantal**	**Eenheid**	**Prijs per eenheid**	**Afschrijftermijn**	**Totaal**
koelmachine	1	1	€ 163,200.00	10	€ 163,200.00
Ketel	1	1	€ 106,800.00	10	€ 106,800.00
					€ -
					€ -
					€ -
					€ -
					€ -
Totaal					**€ 270,000.00**
Voorbereidingskosten	Kunnen, afhankelijk van situatie, ook gefinancierd worden				
Omschrijving	**Aantal**	**Eenheid**	**Prijs per eenheid**		**Totaal**
Ontwerp etc directie etc	1	uur	€ 13,500.00		€ 13,500.00
					€ -
					€ -
					€ -
					€ -
					€ -
					€ -
Totaal					**€ 13,500.00**

Figure 33: Investments Conventional

Totaal					€ 1,126,800.00
Investeringskosten					
Omschrijving	**Aantal**	**Eenheid**	**Prijs per eenheid**	**Afschrijftermijn**	**Totaal**
wko bronnen	1	1	€ 620,000.00	40	€ 620,000.00
WP	1	2	€ 250,000.00	20	€ 250,000.00
ketel	1	1	€ 106,800.00	10	€ 106,800.00
bronpomp	2	1	€ 15,000.00	10	€ 30,000.00
					€ -
					€ -
					€ -
Totaal					**€ 1,006,800.00**
Voorbereidingskosten	Kunnen, afhankelijk van situatie, ook gefinancierd worden				
Omschrijving	**Aantal**	**Eenheid**	**Prijs per eenheid**		**Totaal**
Ontwerp etc directie etc	1000	uur	€ 120.00		€ 120,000.00
					€ -
					€ -
					€ -
					€ -
					€ -
					€ -
Totaal					**€ 120,000.00**

Figure 34: Investments Doublet

Totaal					€ 2,994,444.14
Investeringskosten					
Omschrijving	**Aantal**	**Eenheid**	**Prijs per eenheid**	**Afschrijftermijn**	**Totaal**
bronnen	1	1	€ 862,000.00	40	€ 862,000.00
pompen	3	1	€ 20,000.00	10	€ 60,000.00
zonnecollectoren	1	1	€ 1,843,644.14	30	€ 1,843,644.14
DK	1	1	€ 108,800.00	10	€ 108,800.00
					€ -
					€ -
					€ -
Totaal					**€ 2,874,444.14**
Voorbereidingskosten	Kunnen, afhankelijk van situatie, ook gefinancierd worden				
Omschrijving	**Aantal**	**Eenheid**	**Prijs per eenheid**		**Totaal**
Ontwerp etc directie etc	1000	uur	€ 120.00		€ 120,000.00
					€ -
					€ -
					€ -
					€ -
					€ -
					€ -
Totaal					**€ 120,000.00**

Figure 35: Investments Triplet

7.2 Appendix B

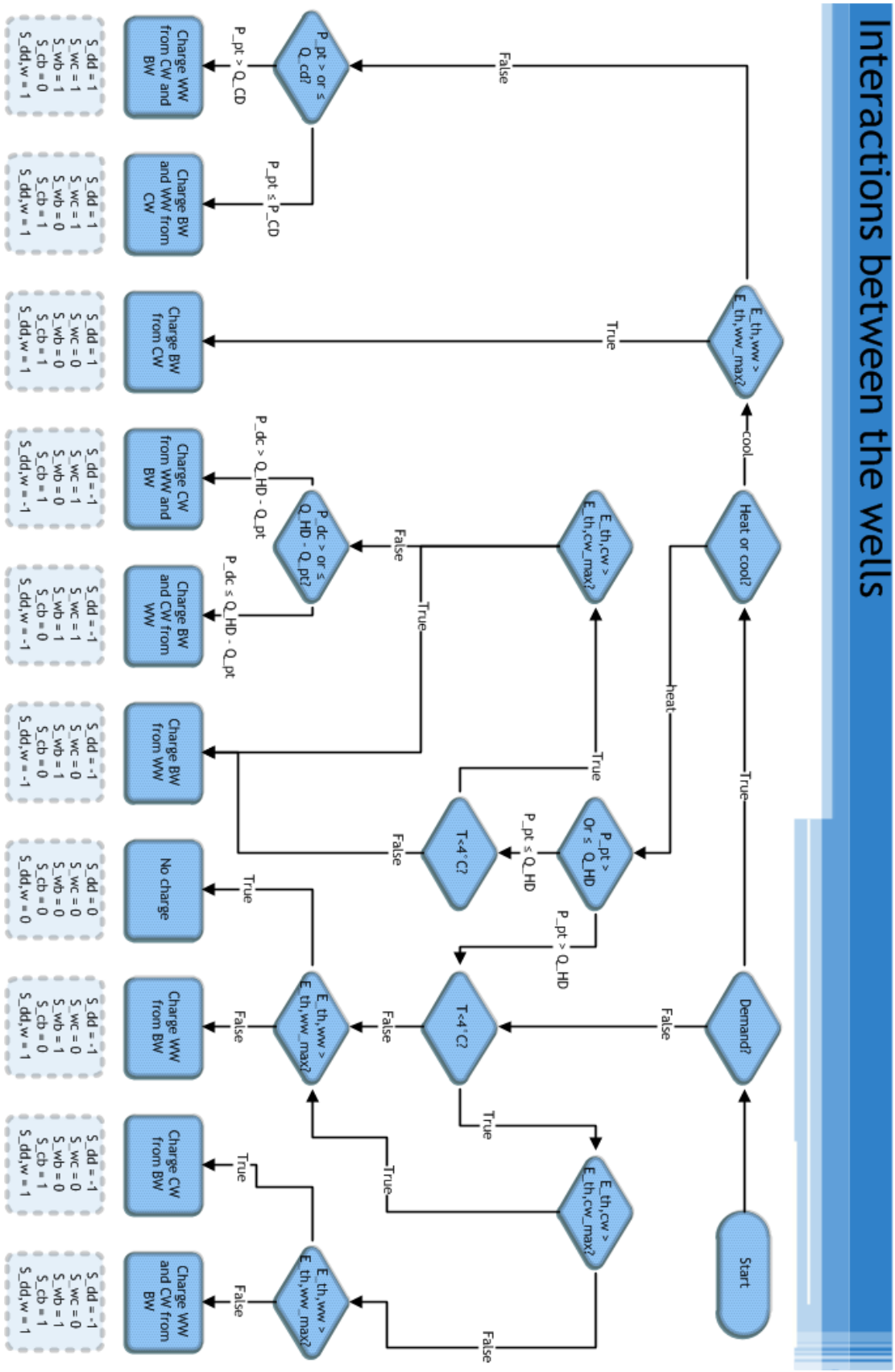

Figure 36: Flowchart of fluxes between the storages

7.3 Appendix C

$$dV_W^{i-1} = \frac{1+s_{dd}^{i-1}}{2} s_{wc}^{i-1} \left(\frac{\mathrm{s}_{\mathrm{wb}}^{\mathrm{i-1}} Q_{CD}^{i-1}}{C_w \cdot \left| T_{aq,dem_{out}}^{i-1} - T_{aq,C}^{i-1} \right|} - \frac{\mathrm{s}_{\mathrm{wb}}^{\mathrm{i-1}} Q_{CD}^{i-1} \frac{\left| T_{aq,dem_{out}}^{i-1} - T_{aq,w_{in}}^{i-1} \right|}{\left| T_{aq,dem_{out}}^{i-1} - T_{aq,C}^{i-1} \right|} - Q_{pt}^{i-1}}{C_w \cdot \left| T_{aq,W_{in}}^{i-1} - \mathrm{s}_{\mathrm{cb}}^{\mathrm{i-1}} T_{aq,dem_{out}}^{i-1} - \mathrm{s}_{\mathrm{wb}}^{\mathrm{i-1}} T_{aq,b}^{i-1} \right|} \right)$$
$$+ \frac{1-s_{dd}^{i-1}}{2} \left(\left(\frac{\mathrm{s}_{\mathrm{wc}}^{\mathrm{i-1}} + \mathrm{s}_{\mathrm{wb}}^{\mathrm{i-1}}}{1 + s_{wc}^{i-1} \mathrm{s}_{\mathrm{wb}}^{\mathrm{i-1}}} \right) \left(\frac{Q_{pt}^{i-1} - Q_{HD}^{i-1}}{C_w \cdot \left| \frac{1+s_{dd,w}^{i-1}}{2} (T_{aq,W_{in}}^{i-1} - T_{aq,b}^{i-1}) + \frac{1-s_{dd,w}^{i-1}}{2} (T_{aq,w}^{i-1} - T_{aq,dem_{out}}^{i-1}) \right|} \right) \right) \quad (23)$$

$$dV_B^{i-1} = \frac{1+s_{dd}^{i-1}}{2} \left(\frac{s_{cb}^{i-1} Q_{CD}^{i-1}}{C_w \cdot \left| T_{aq,dem_{out}}^{i-1} - T_{aq,C}^{i-1} \right|} + \frac{s_{wb}^{i-1} Q_{CD}^{i-1} \frac{\left| T_{aq,dem_{out}}^{i-1} - T_{aq,w_{in}}^{i-1} \right|}{\left| T_{aq,dem_{out}}^{i-1} - T_{aq,C}^{i-1} \right|} - s_{wc}^{i-1} Q_{pt}^{i-1}}{C_w \cdot \left| T_{aq,W_{in}}^{i-1} - \mathrm{s}_{\mathrm{cb}}^{\mathrm{i-1}} T_{aq,dem_{out}}^{i-1} - \mathrm{s}_{\mathrm{wb}}^{\mathrm{i-1}} T_{aq,b}^{i-1} \right|} \right)$$
$$+ \frac{1-s_{dd}^{i-1}}{2} \left(\frac{s_{wc}^{i-1} + s_{cb}^{i-1}}{1 + s_{wc}^{i-1} s_{cb}^{i-1}} \left(\frac{s_{wc}^{i-1} s_{cb}^{i-1} \frac{\left(Q_{HD}^{i-1} - Q_{pt}^{i-1}\right) \cdot \left| T_{aq,dem_{out}}^{i-1} - T_{aq,c_{in}}^{i-1} \right|}{\left| T_{aq,w}^{i-1} - T_{aq,dem_{out}}^{i-1} \right|} - Q_{dc}^{i-1}}{C_w \cdot \left| \mathrm{s}_{\mathrm{cb}}^{\mathrm{i-1}} (T_{aq,C_{in}}^{i-1} - T_{aq,b}^{i-1}) + \left(1 - \mathrm{s}_{\mathrm{cb}}^{\mathrm{i-1}}\right) (T_{aq,dem_{out}}^{i-1} - T_{aq,c_{in}}^{i-1}) \right|} \right) \right.$$
$$\left. + \mathrm{s}_{\mathrm{wb}}^{\mathrm{i-1}} \left(\frac{Q_{HD}^{i-1} - Q_{pt}^{i-1}}{C_w \cdot \left| \frac{1+s_{dd,w}^{i-1}}{2} (T_{aq,W_{in}}^{i-1} - T_{aq,b}^{i-1}) + \frac{1-s_{dd,w}^{i-1}}{2} (T_{aq,w}^{i-1} - T_{aq,dem_{out}}^{i-1}) \right|} \right) \right) \quad (24)$$

$$dV_C^{i-1} = -\frac{1+s_{dd}^{i-1}}{2} \frac{Q_{CD}^{i-1}}{C_w \cdot \left| T_{aq,dem_{out}}^{i-1} - T_{aq,C}^{i-1} \right|}$$
$$+ \frac{1-s_{dd}^{i-1}}{2} \frac{s_{wc}^{i-1} + s_{cb}^{i-1}}{1 + s_{wc}^{i-1} s_{cb}^{i-1}} \left(s_{wc}^{i-1} s_{cb}^{i-1} \frac{Q_{HD}^{i-1} - Q_{pt}^{i-1}}{C_w \cdot \left| T_{aq,w}^{i-1} - T_{aq,dem_{out}}^{i-1} \right|} \right.$$
$$\left. - \frac{s_{wc}^{i-1} s_{cb}^{i-1} \frac{\left(Q_{HD}^{i-1} - Q_{pt}^{i-1}\right) \cdot \left| T_{aq,dem_{out}}^{i-1} - T_{aq,c_{in}}^{i-1} \right|}{\left| T_{aq,w}^{i-1} - T_{aq,dem_{out}}^{i-1} \right|} - Q_{dc}^{i-1}}{C_w \cdot \left| \mathrm{s}_{\mathrm{cb}}^{\mathrm{i-1}} (T_{aq,C_{in}}^{i-1} - T_{aq,b}^{i-1}) + \left(1 - \mathrm{s}_{\mathrm{cb}}^{\mathrm{i-1}}\right) (T_{aq,dem_{out}}^{i-1} - T_{aq,c_{in}}^{i-1}) \right|} \right) \quad (25)$$

$$T_{aq,w}^{i} = \frac{V_{WW}^{i-1} \cdot T_{aq,w}^{i-1} + \left(\left(\frac{1+s_{dd}^{i-1}}{2} \right) \mathrm{s}_{\mathrm{wc}}^{\mathrm{i-1}} + \left(\frac{1-s_{dd}^{i-1} s_{dd,w}^{i-1}}{2} \right) \mathrm{s}_{\mathrm{wb}}^{\mathrm{i-1}} \right) * dV_W^{i-1} * T_{aq,w_{in}}^{i-1} - \alpha * (T_{aq,w}^{i-1} - T_{aq,amb})}{V_{WW}^{i-1} + \left(\left(\frac{1+s_{dd}^{i-1}}{2} \right) \mathrm{s}_{\mathrm{wc}}^{\mathrm{i-1}} + \left(\frac{1-s_{dd}^{i-1} s_{dd,w}^{i-1}}{2} \right) \mathrm{s}_{\mathrm{wb}}^{\mathrm{i-1}} \right) * dV_W^{i-1}} \quad (26)$$

$$T_{aq,b}^{i} = \frac{V_{BW}^{i-1} \cdot T_{aq,b}^{i-1} + \left(\frac{1+s_{dd}^{i-1}}{2} s_{cb}^{i-1} + \frac{1-s_{dd}^{i-1}}{2} \frac{1-s_{dd,w}^{i-1}}{2} s_{wb}^{i-1} \right) \cdot dV_B^{i-1} T_{aq,b_{in}}^{i-1} - \alpha * \left(T_{aq,b}^{i-1} - T_{aq,amb} \right)}{V_{BW}^{i-1} + \left(\frac{1+s_{dd}^{i-1}}{2} s_{cb}^{i-1} + \frac{1-s_{dd}^{i-1}}{2} \frac{1-s_{dd,w}^{i-1}}{2} s_{wb}^{i-1} \right) \cdot dV_B^{i-1}} \quad (27)$$

$$T_{aq,c}^{i} = \frac{V_{CW}^{i-1} \cdot T_{aq,c}^{i-1} + \frac{1-s_{dd}^{i-1}}{2} \left(\frac{\mathrm{s}_{\mathrm{wc}}^{\mathrm{i-1}} + s_{cb}^{i-1}}{1 + s_{wc}^{i-1} \mathrm{s}_{\mathrm{cb}}^{\mathrm{i-1}}} \right) \cdot dV_C^{i-1} T_{aq,c_{in}}^{i-1} - \alpha * \left(T_{aq,c}^{i-1} - T_{aq,amb} \right)}{V_{CW}^{i-1} + \frac{1-s_{dd}^{i-1}}{2} \left(\frac{\mathrm{s}_{\mathrm{wc}}^{\mathrm{i-1}} + s_{cb}^{i-1}}{1 + s_{wc}^{i-1} \mathrm{s}_{\mathrm{cb}}^{\mathrm{i-1}}} \right) \cdot dV_C^{i-1}} \quad (28)$$

$$Q_w^{i-1} = \frac{1 + s_{dd}^{i-1}}{2} \cdot C_w \cdot dV_W^{i-1} \cdot \left|T_{aq,w_{in}}^{i-1} - T_{ref,w}\right| + \frac{1 - s_{dd}^{i-1}}{2} C_w dV_W^{i-1} \left(\frac{1 - s_{dd,w}^{i-1}}{2} \cdot \frac{\left(s_{wb}^{i-1} + s_{wc}^{i-1}\right)}{1 + s_{wc}^{i-1} s_{wb}^{i-1}} \left|T_{aq,dem_{out}}^{i-1} - T_{aq,w}^{i-1}\right| + \frac{1 + s_{dd,w}^{i-1}}{2} \left(s_{wb}^{i-1} + s_{wc}^{i-1}\right) \left|T_{aq,w_{in}}^{i-1} - T_{ref,w}\right| \right) \quad (29)$$

$$Q_b^{i-1} = \frac{1 + s_{dd}^{i-1}}{2} \cdot C_w \cdot dV_B^{i-1} \left(s_{cb}^{i-1} \left|T_{aq,b_{in}}^{i-1} - T_{ref,b}\right| + \frac{s_{wb}^{i-1}\left(1 + s_{wc}^{i-1}\right)}{1 + s_{wc}^{i-1} s_{wb}^{i-1}} \left|T_{aq,W_{in}}^{i-1} - T_{aq,b}^{i-1}\right| \right) + \frac{1 - s_{dd}^{i-1}}{2} \cdot C_w \cdot dV_B^{i-1} \left(\frac{1 - s_{dd,w}^{i-1}}{2} s_{wb}^{i-1} \left|T_{aq,b_{in}}^{i-1} - T_{ref,b}\right| + \frac{1 + s_{dd,w}^{i-1}}{2} \left(s_{wb}^{i-1} - s_{cb}^{i-1}\right) \left|T_{aq,w_{in}}^{i-1} - T_{aq,b}^{i-1}\right| + \left(\frac{s_{cb}^{i-1}\left(1 + s_{wc}^{i-1}\right)}{1 + s_{wc}^{i-1} s_{cb}^{i-1}} - s_{wb}^{i-1} \right) \left|T_{aq,C_{in}}^{i-1} - T_{aq,b}^{i-1}\right| \right) - \frac{1 - s_{dd}^{i-1}}{2} s_{wb}^{i-1} s_{cb}^{i-1} C_w \left(dV_C^{i-1} \left|T_{aq,C_{in}}^{i-1} - T_{aq,b}^{i-1}\right| + dV_w^{i-1} \left|T_{aq,w_{in}}^{i-1} - T_{aq,b}^{i-1}\right| \right) \quad (30)$$

$$Q_c^{i-1} = \frac{1 - s_{dd}^{i-1}}{2} \cdot C_w \cdot dV_C^{i-1} \cdot \left|T_{aq,c_{in}}^{i-1} - T_{ref,c}\right| + \frac{1 + s_{dd}^{i-1}}{2} \cdot C_w \cdot dV_c^{i-1} \cdot \left|T_{aq,dem_{out}}^{i-1} - T_{aq,c}\right| \quad (31)$$

7.4 Appendix D

7.4.1 Temperature representation

An alternative method, called the ϕ-step method, can be used to represent the thermal losses in the triplet model. The convergence towards ambient groundwater temperature in this method is described by a step function, called the ϕ-step function. In this method the storage temperature is equal to the injection temperature at the well as long as there is warm water injected. When water is extracted and the extracted volume reaches a certain fraction ϕ of the injected volume, the temperature steps to the ambient groundwater temperature and the storage volume is reset. What the fraction ϕ is, is empirically determined from Figure 16c.

7.4.2 Comparing to α-method

The reference scenario is used as an example for the implementation of the ϕ-step method in the triplet model for the warm storage. The results are calculated by making use of CM2 and are shown in Figure 37b, where the discrepancy between the temperature representation for the triplet and subsurface model is observed. In Figure 37a the temperature discrepancy is shown for the α-method. Both methods show that for the warm storage, the discrepancy between the subsurface and triplet model outputs is the largest. However, for the cold and buffer storage – i.e. for lower storage temperatures – the temperature losses are relatively well described by making use of the α-method. This coincides with previous work by (Rostampour et al. 2016) and therefore the α-method was chosen to represent the temperature and thermal losses of the storages in the triplet model. Additional research is necessary to provide a more supported approach for the ϕ-step method.

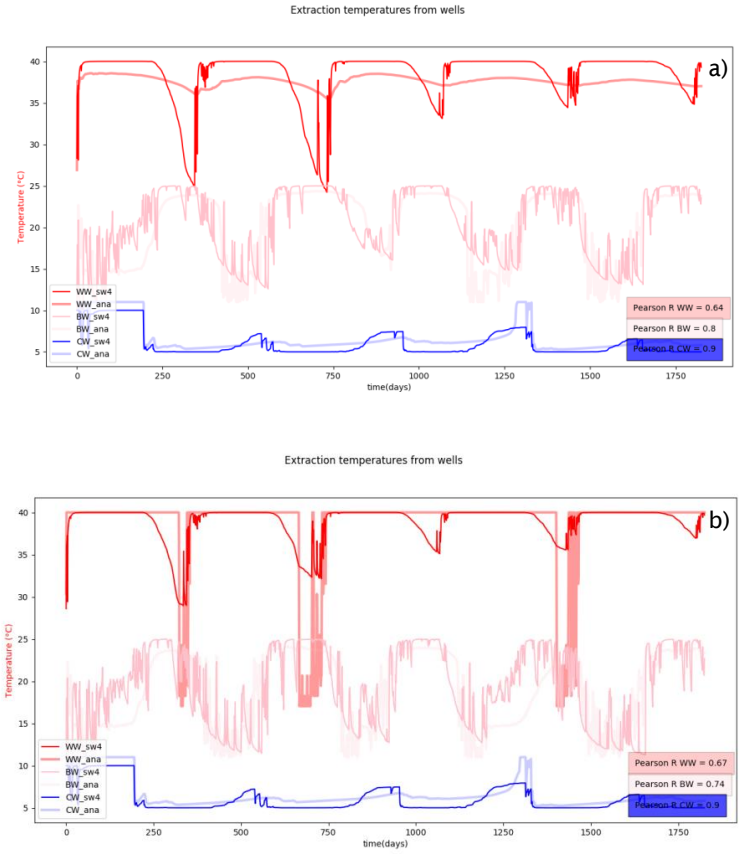

Figure 37: Daily average temperature profiles of the warm(red lines), buffer(pink lines) and cold storages (blue lines) over 5 years. The sharp lines indicate the subsurface outputs, the bold transparent lines indicate the analytic outputs. Pearson's R, is presented in order to quantify the correspondence between the analytic and subsurface outputs. **a):** Temperatures modeled with α-method. **b):** Temperature of warm storage modeled with ϕ-step function.

8 References

Bloemendal, IR. Martin, and Niels Hartog. 2016. "After the booml evaluation of dutch ates-systems for energy efficiency." In *European Geothermal Congress 2016*. Strassbourg, France.
Bloemendal, IR. Martin, Marc Jaxa-Rozen, and Vahab Rostampour. 2017. "Improved performance of Heat Pumps helps to use full potential of subsurface space for Aquifer Thermal Energy Storage." In *Heat pump conference*. Rotterdam.
Bloemendal, Martin, and Hetty Mathijssen. 2013. "Cahier Bodemenergie." In.
Bloemendal, Martin, Theo Olsthoorn, and Frans van de Ven. 2015. 'Combining climatic and geo-hydrological preconditions as a method to determine world potential for aquifer thermal energy storage', *Science of the Total Environment*, 538: 621-33.
Christenson, M, H Manz, and D Gyalistras. 2006. 'Climate warming impact on degree-days and building energy demand in Switzerland', *Energy Conversion and Management*, 47: 671-86.
De Rosa, Mattia, Vincenzo Bianco, Federico Scarpa, and Luca A Tagliafico. 2014. 'Heating and cooling building energy demand evaluation; a simplified model and a modified degree days approach', *Applied energy*, 128: 217-29.
Dekker. 2016. 'Bepalende factoren voor een goed functionerende WKO', *Kennisplatform bodemenergie*.
Delft, FMVG TU. 2013. 'TU Delft Energy monitor', TU Delft, Accessed 03-05. http://energymonitor.tudelft.nl/Home.
Drijver, Benno. 2013. "Meer met bodemenergie, hogetemperatuursopslag." In.: Bioclear, Deltares, IF Technology

en Wageningen Universiteit.
Evans, Tony. 2012. 'The different technologies for cooling data centers', *APC white paper*, 59.
Hacking, Tim. 2017. 'The suitability of a high temperature aquifer thermal energy storage on the TU-Delft campus', Bachelor thesis, TU-Delft.
INMET. 2017. "São Paulo, (Mirante de Santana)." In.
IPCC. 2011. 'IPCC special report on renewable energy sources and climate change mitigation'.
Jan Hofman, Edwin de Buijzer, Jeroen Nagel, and Wim van Houdt. 2015. "ENERGIE, WATER EN AFVAL: DUURZAME OPTIES VOOR NIEUW ZIEKENHUIS TERGOOI." In.: h2o water netwerk.
Kakac, Sadik, Hongtan Liu, and Anchasa Pramuanjaroenkij. 2012. *Heat exchangers: selection, rating, and thermal design* (CRC press).
KNMI. n.d. 'Daggegevens van het weer in Nederland', Minesterie van infrastructuur en millleu, Accessed 05-2017. https://www.knmi.nl/nederland-nu/klimatologie/daggegevens.
Langevin, Christian D., Jr. Daniel T. Thorne, Alyssa M. Dausman, Michael C. Sukop, and Weixing Guo. 2008. 'SEAWAT Version 4: A Computer Program for Simulation

of Multi-Species Solute and Heat Transport.' in U.S. Geological Survey (ed.), *Techniques and Methods Book 6* (U.S. Geological Survey: Reston, Virginia).
Lee, Kun Sang. 2010. 'A review on concepts, applications, and models of aquifer thermal energy storage systems', *Energies*, 3: 1320-34.
———. 2013. 'Underground thermal energy storage.' in, *Underground Thermal Energy Storage* (Springer).
Lucas, M, PJ Martinez, and A Viedma. 2008. 'Comparative experimental drift study between a dry and adiabatic fluid cooler and a cooling tower', *international journal of refrigeration*, 31: 1169-75.
Martin Bloemendal, Edwin de Buijzer, Ilse Laura Snip, Pieterse-Quirijns, Claudia Agudelo-Vera, Annemieke van Doorn, and Marcel Paalman. 2016. "Innovatieve oplossingen energie- & waterketen Lelystad Airport en Lelystad Airport Businesspark." In.: KWR research cycle institute.
Mathioulakis, Emmanouil, and Vassilis Belessiotis. 2002. 'A new heat-pipe type solar domestic hot water system', *Solar Energy*, 72: 13-20.
Meijer, P.H., and R Verweij. 2009. "Energieverbruik per functie voor SenterNovem " In.: Meijer Energie & Milieumanagement B.V. .
Paksoy, HO, O Andersson, S Abaci, H Evliya, and B Turgut. 2000. 'Heating and cooling of a hospital using solar energy coupled with seasonal thermal energy storage in an aquifer', *Renewable energy*, 19: 117-22.
Pérez-Lombard, Luis, José Ortiz, and Christine Pout. 2008. 'A review on buildings energy consumption information', *Energy and buildings*, 40: 394-98.

Rijksoverheid. 2016. "Energieagenda." In *Naar een CO_2 -arme energievoorziening*. Ministerie van Economische Zaken.

Rostampour, Vahab, Martin Bloemendal, Marc Jaxa-Rozen, and Tamas Keviczky. 2016. "A control-oriented model for combined building climate comfort and aquifer thermal energy storage system." In *European Geothermal Congress*. Strassbourg, France.

Rostampour, Vahab, Martin Bloemendal, and Tamas Keviczky. 2017. "A model predictive framework of ground source heat pump coupled with aquifer thermal energy storage system in heating and cooling equipment of a building." In *heat pump conference*. Rotterdam: IEA energy technology network.

SMHI. 2017. "Meteorolgiska observationer Umea (Sweden)." In, edited by SMHI.

Sommer, Wijbrand, Johan Valstar, Ingo Leusbrock, Tim Grotenhuis, and Huub Rijnaarts. 2015. 'Optimization and spatial pattern of large-scale aquifer thermal energy storage', *Applied energy*, 137: 322-37.

ThermoKey. n.d. "Heat Exchange Solutions." In.

Thorne, Danny, Christian D Langevin, and Michael C Sukop. 2006. 'Addition of simultaneous heat and solute transport and variable fluid viscosity to SEAWAT', *Computers & Geosciences*, 32: 1758-68.

Umwelt, Bayerisches Landesamt für. 2013. 'Gewässerkundlicher Dienst Bayern', Accessed 05-20017. http://gkd.bayern.de/meteo/karten/index.php?thema=gkd&rubrik=meteo&produkt=n.

van Lopik, Jan H, Niels Hartog, and Willem Jan Zaadnoordijk. 2016. 'The use of salinity contrast for density difference compensation to improve the thermal recovery efficiency in high-temperature aquifer thermal energy storage systems', *Hydrogeology Journal*, 24: 1255-71.

Wei, Lingjiao, Dazhong Yuan, Dawei Tang, and Bangxian Wu. 2013. 'A study on a flat-plate type of solar heat collector with an integrated heat pipe', *Solar Energy*, 97: 19-25.